NASA CONTRACTOR REPORT

CR-22

CR-22

4/2p.

N64 12912

CODE-1

FIELD-EMISSION INVESTIGATION OF THERMAL DESORPTION AND SURFACE DIFFUSION OF CESIUM ON TUNGSTEN

by L. W. Swanson, R. W. Strayer, F. M. Charbonnier, and E. C. Cooper

Jan 1964 42p

Prepared under Contract No. NASw-458 by
FIELD EMISSION CORPORATION
McMinnville, Oregon
for

NATIONAL AERONAUTICS AND SPACE ADMINISTRATION • WASHINGTON, D. C. • JANUARY 1964

(NASA CR-22)

OTS: $1.25

FIELD-EMISSION INVESTIGATION OF THERMAL DESORPTION AND SURFACE DIFFUSION OF CESIUM ON TUNGSTEN

By L. W. Swanson, R. W. Strayer, F. M. Charbonnier, and E. C. Cooper

Field Emission Corporation
McMinnville, Oregon

NATIONAL AERONAUTICS AND SPACE ADMINISTRATION

For sale by the Office of Technical Services, Department of Commerce, Washington, D.C. 20230 -- Price $1.25.

FIELD-EMISSION INVESTIGATION OF THERMAL DESORPTION AND SURFACE DIFFUSION OF CESIUM ON TUNGSTEN

SUMMARY

12912

Thermal desorption and surface diffusion of cesium coatings on a tungsten substrate have been investigated by pulsed-field-emission microscopy.

Measured values of the heat of desorption for neutral cesium atoms vary with cesium coverage from 18 kilocalories per mole at 1.0 monolayer of cesium to 69 kilocalories per mole as the degree of coverage approaches zero. Electric-field strengths up to 13 megavolts per centimeter had negligible effect, within experimental error, on the heat of neutral desorption at zero coverage. An average heat of desorption for cesium ions of 55 kilocalories per mole is obtained for the range of coverage from 0 to 0.07 monolayer.

Measured values of the surface-diffusion activation energy range from 6 to 17 kilocalories per mole depending on the degree of coverage and the crystallographic orientation of the substrate under the condition of zero electric field at the surface. Application of d-c fields of either polarity (ranging from 14 to -22 Mv/cm) is found to produce a significant decrease in the activation energy for surface diffusion. A tentative explanation of this effect is given.

In the interpretation of the data, use is made of the detailed information available by examination of the field-emission-microscope patterns.

AUTHOR

INTRODUCTION

This report concerns a study recently undertaken at the Field Emission Corporation Research Laboratory of the familiar problem of the behavior of alkali metal layers on metal substrates with present emphasis on the cesium-on-tungsten system. The novelty of the present work stems largely from a choice of experimental techniques based on field electron emission that are designed to complement other investigations by permitting measurements under experimental conditions not readily studied by other techniques. The main objective of the present work is to contribute to the fundamental knowledge and understanding of the behavior of alkali layers on metal substrates. A specific practical motivation of

the work is provided by the desire to understand and prevent voltage breakdown between cesium-covered electrodes at the high voltage gradients required for effective operation of ion propulsion engines.

The behavior of cesium atoms on a tungsten surface has been studied most extensively by Langmuir and Taylor. Using thermionic techniques, they investigated the surface mobility of cesium on tungsten (ref. 1) and the evaporation of atoms, ions, and electrons from a cesium-coated tungsten surface as a function of the degree of cesium coverage and the surface temperature (ref. 2).

The behavior of cesium on tungsten is, of course, complicated by the fact that tungsten has a crystalline structure and is therefore anisotropic, so that quantities of fundamental interest such as substrate work function, cesium binding energy, and surface migration rates depend on the crystallographic orientation of the substrate. To obtain greater detail and to ascertain the magnitude of this effect, several investigators (refs. 3 to 5) have used various forms of the thermionic-emission-projection microscope to investigate the dependence of adsorption and/or evaporation of cesium atoms on the crystallographic orientation of the substrate.

In space technology, cesium finds its most important uses in the areas of thermionic converters and ion engines. However, the operating conditions are fundamentally different in these two cases. Thermionic converters are characterized by elevated electrode temperatures, low voltage gradients at the electrode surfaces, and a cesium surface layer that is in equilibrium with the cesium vapor present at relatively high pressure in the gap between the electrodes. On the contrary, ion engines are characterized, in general, by a relatively high vacuum, high voltage gradients at the electrode surfaces, and electrode temperatures that may be low enough to preclude both thermionic emission and evaporation of cesium atoms or ions at an appreciable rate.

With this in mind, it is readily seen that the previous techniques based on thermionic emission (refs. 1 to 5) can best duplicate those conditions found in thermionic converters and are therefore well suited to investigations pertaining to these devices. These techniques, however, are not readily applicable to a study of conditions prevailing in the accelerator systems of ion engines. Fortunately, the methods of field-emission microscopy, and particularly the recent extension in reference 6 of these methods in the embodiment of the pulsed-field or T-F emission-projection microscope, are ideally suited to the present problem and have been selected for this reason.

In the area of field emission, preliminary work has been done in an investigation of the dependence of the work function of cesium-coated tungsten on the degree of cesium coverage (ref. 7). This research was sponsored by the National Aeronautics and Space Administration through the office of Grants and Research Contracts.

EXPERIMENTAL METHODS

Pulsed-Field-Emission-Projection Microscopy

The main experimental tool used so far in the present study of surface diffusion and desorption rates is a special version illustrated in figure 1 of the field-emission-projection microscope (FEPM) first introduced by the authors of reference 8. General discussions of field-emission microscopy have been published (refs. 9 to 11). Details on construction and processing have been presented in the literature (refs. 6 and 12). Briefly, the FEPM is a diode in which field emission is drawn from the single-crystal hemispherical tip of a very sharp needle (tip radius usually $<1\mu$) mounted at the center of an evacuated spherical bulb coated with a phosphor. When a sufficiently positive "viewing voltage" is applied to the phosphor screen, electrons are emitted by tunneling through the potential barrier at the emitter surface; this process, called field or T-F emission, depending on the tip temperature, can be made to occur at all temperatures to absolute zero. The field-emitted electrons travel along nearly radial paths and form a visible field-emission pattern on the phosphor screen that provides a highly magnified emission image of the tip surface. The FEPM is characterized by a high magnification (approximately equal to the ratio of screen to tip radius, typically in the 10^5 to 10^6 power range), a high resolving power for smooth surfaces (typically 30 A, limited by the initial energy spread of about 0.25 ev of the field-emitted electrons) and a still higher resolving power (2.2 A in certain cases) for surface irregularities. Pattern detail arises from local variations in field and work function at the tip surface, and the pattern has a symmetry characteristic of the crystal structure of the tip material. Observation of the emission pattern of the uncoated tip provides a sensitive criterion for checking the smoothness and cleanliness of the substrate prior to deposition of the alkali adsorbate.

The presence, migration, and desorption of an adsorbate such as cesium are detected and measured through observation of the occurrence and time rate of resulting changes in the field-emission pattern that permit a determination of the associated physical constants (sticking probability, rate constant, and activation energies). However, at the high values of applied voltage gradients required for field emission, there is a possibility that the large electrostatic forces accompanying steady-state fields may alter the processes under study and, at high temperatures, may even alter the shape of the substrate. To avoid this reaction, the high "viewing field" required for field emission may be applied in the form of very short pulses at low duty factor (e.g., 1-μsec pulses at a rate of 30 pulses/sec), and the emission pattern is then viewed as a motion picture. This technique, introduced in reference 6, minimizes the perturbing effect of the viewing field on the event under study (in the experiment to follow this has been verified by checking the insensitivity of the results to a change in the duty factor and to a change in pulse voltage) and allows almost complete freedom in the selection both of the tip temperature and of the magnitude and polarity of the d-c voltage gradient, which may be applied at the tip (in addition to the pulsed viewing field).

Experimental Tube

The modified FEPM tube used in these investigations underwent several changes in design before a model satisfactory in all respects was obtained. The tube, illustrated in figure 1, used to obtain most of the data given subsequently consists of a cesium reservoir, a cesium evaporation platform, and an FEPM arrangement.

The cesium reservoir is a small cesium-containing glass ampule with a breakoff seal. The ampule is obtained in the following manner: The cesium is purchased from the supplier in partly evacuated (to about 1 torr pressure of an inert gas, probably argon) glass ampules, each containing about 1 gram of pure (99.9 percent) cesium. One of these commercial ampules is placed in a copper tube that is fastened to a glass manifold connecting to five or six breakoff-seal ampules and a high-vacuum system. After the system is evacuated and baked for 12 hours at 500° C, the glass ampule containing the cesium is broken by crushing the copper tube and allowing the inert gas to be pumped away. When the vacuum has returned to less than 10^{-8} torr, the cesium is slowly distilled into the breakoff-seal ampules. These are sealed off and attached to experimental tubes as needed. The breakoff-seal ampule is broken as a last step before sealoff during evacuation of an experimental tube. During this step no change in pressure in the experimental tube is observed by monitoring the field-emission current in the tube or by reading the pressure of the ion gage attached to the vacuum system.

Of the several methods of obtaining a controllable cesium source, the platinum platform, illustrated in figure 1, has proved to be the most satisfactory, because a large number of reproducible doses are obtainable from one loading of the platform. After breaking the seal of the cesium-containing ampule connected to the sidearm, the cesium is heated by an external Nichrome heater and condensed on the platform, which is maintained at 77° K by filling the Teflon sleeve with liquid nitrogen. To eliminate cesium distillation into the main body of the tube during the loading of the source, a nickel disk is positioned over the aperture; the disk can be removed magnetically. Subsequently, controlled amounts of cesium can be evaporated from the platform onto the emitter tip by heating the platform to a known temperature for a fixed length of time. In the experiments described herein, the reproducibility of the amount of cesium evaporated onto the tip was checked by measuring the corresponding change in work function of the emitter surface and by observing its field-emission pattern. This value was found to be within 5 percent, which was sufficient for the present purpose.

The construction of the FEPM part of the experimental tube is standard (refs. 11 and 12) except for provision made to measure and control the emitter temperature (ref. 13). The tip temperature is derived from an accurate measurement of the resistance of a small section of the emitter supporting filament. This measurement utilizes the fact that the resistivity of tungsten is a well-known, monotonic, and nearly linear function of temperature over the range of interest. The resistance of a segment of the loop is determined by passing an accurately known d-c current through it and measuring the potential difference across it by means of two small leads attached to the filament. The resistance is calibrated by measurement at several well-determined temperatures.

Procedure

After the experimental tube is evacuated and the platform source is loaded, the tube is then placed in a large Dewar containing liquid nitrogen, which prevents cesium migration and achieves a high degree of vacuum ($\sim 10^{-12}$ torr). The Dewar has a window through which the field-emission pattern of the tube can be viewed. The tube is kept at liquid-nitrogen temperature for all subsequent experiments.

To measure migration and desorption rates accurately at a given temperature, the temperature of the tip is raised quickly (within a few seconds) from liquid-nitrogen temperature to the desired value and held constant for the chosen heating period by means of a filament temperature regulator (ref. 11), which controls the resistance of a segment of the filament supporting the tip.

To determine the values of electric field at the emitter surface, the geometrical ratio β of the electric field at the tip apex to the applied screen voltage must be known. The quantity β can be determined from the measured relation between field-emitted current and applied screen voltage for the clean tungsten tip ($\varphi_{av} = 4.52$ ev).

In a typical experiment, the tungsten tip is first cleaned by brief heating at approximately 2400° K, then cooled to liquid-nitrogen temperature. Cesium is then evaporated onto the portion of the tip facing the source, and the degree of coverage on the tip is determined from its work function by using Langmuir's data to relate work function to degree of coverage (ref. 2) (see the following section). The tip temperature and/or the d-c voltage gradient at the tip surface is then increased to the desired value, and the progress of cesium migration or evaporation is determined through a recording of the successive field-emission patterns and of the peak screen viewing voltage required to maintain a constant peak field-emitted current from the tip. Observation of the shape of the moving boundary of the cesium-covered region permits a rough comparison of surface migration rates for different crystallographic orientations of the substrate. The activation energy for surface migration and its dependence on the crystallographic orientation of the substrate are obtained from Arrhenius plots ($\ln t$ against $1/T$) (ref. 14) of the time t taken for the boundary to move from one selected reference position to another. (Ref. 14 gives a general review of the terms of first-order reaction-rate theory.) The cesium evaporation rates as a function of temperature and field are obtained by deriving the time rate of change of the work function, which is itself obtained through the field-emission law from experimental current-voltage data.

WORK-FUNCTION DETERMINATIONS

The work function of the emitting surface is used in this study to estimate the degree of cesium coverage of the coated surface.

The field-emission method of determining the work function is based on the well-known and experimentally confirmed Fowler-Nordheim law of field emission (ref. 9), which may be written in terms of the directly measurable field-emission current I and applied voltage V as

$$I = A'V^2 \exp\left[-\frac{10^4 m}{V}\right] \tag{1}$$

where A' is the intercept and m is the slope of a Fowler-Nordheim plot of the current and voltage plotted in the form of $\log I/V^2$ against $10^4/V$. The work function φ is related to m by the Fowler-Nordheim law

$$m = \frac{d\left(\log \frac{I}{V^2}\right)}{d\left(\frac{10^4}{V}\right)} = 2.83 \times 10^{-3} \frac{\varphi^{3/2}}{\beta} \tag{2}$$

over the range of currents used. Absolute determinations of the work function require knowledge of the geometric factor β. For the present study in which β does not change as the emitter is coated with cesium, knowledge of the value of β is not required and, using the work function φ_1 for the clean uncoated emitting surface as a reference, the work function φ_2 of the surface when coated can be determined from

$$\varphi_1 = \varphi_2 \left(\frac{m_2}{m_1}\right)^{2/3} \tag{3}$$

where m_1 and m_2 are the slopes of the corresponding Fowler-Nordheim plots.

The work function of cesium-covered tungsten tips has been measured by this method for a wide range of coverages. First, the field-emission current-voltage characteristic I as a function of V was measured for the clean tungsten emitter (illustrated by the field-emission pattern in fig. 8(a)) immediately after high-temperature heating (>2400° K) of the tip, and the slope m_1 of the corresponding Fowler-Nordheim plot was determined. Second, enough cesium was evaporated onto the tip refrigerated at 77° K and then spread into a smooth layer by low-temperature surface migration to provide an average degree of coverage well above 1.0 monolayer. Then the tip was heated for 60-second intervals to successively higher temperatures T until all the cesium was removed. Following each interval of heating, a work-function determination was made from the slope m_2 of a Fowler-Nordheim plot.

The results of these measurements are shown in figure 2. Starting at point A (low T, high degree of coverage θ, very low work function $\varphi_A = 1.45$ ev), the work function increases to a maximum $\varphi_B = 1.85$ electron volts at 265° K (point B), then decreases to a relative minimum $\varphi_C = 1.60$ electron volts at 310° K (point C), then increases steadily until the cesium is completely evaporated, and the clean tungsten work function $\varphi_D = 4.52$ electron volts is reached at 920° K (point D). The change in work function between points C and D is the same as that observed by Langmuir between the work function of a clean tungsten surface and a minimum work function, which he obtained at 0.67 monolayer (ref. 2). Langmuir's results are replotted in figure 3 and extended to 1.0 monolayer. The value of work function at point B of figure 2 is in good agreement with the value that could be inferred by extrapolation to $\theta = 1$ of Langmuir's data. From this, it is inferred that the measured work functions of this investigation can be related to the degree of cesium coverage by means of

Langmuir's data (fig. 3) for coverages below 1.0 monolayer. This relation is assumed for the remainder of the report.

Also plotted in figure 2 are the emitted current at 780 volts and the logarithm of the pre-exponential factor A' of equation (1) as functions of the temperature to which the tip had been heated. It is interesting to note that the current increases in the range from A to B in which the work function is also increasing. This unusual behavior is explained by the very large increase in A' in this region. The magnitude of the increase in A', however, is not well understood, since A' is a function of the surface properties of the emitter (such as emitting area and work function), which do not vary rapidly.

It is interesting to note that these work-function measurements, by means of field emission at temperatures low enough that a high cesium coverage can be maintained in a high vacuum, indicate that Langmuir's minimum at $\theta = 0.67$ is only a relative minimum, since still lower work-function values are obtained at degrees of coverage greater than 1.0 monolayer. The minimum obtained here at $\theta > 1$ is in reasonable agreement with the minimum work function of 1.36 electron volts obtained earlier by similar field-emission methods (ref. 7). For very high coverages (probably several monolayers) the work function of the surface is found to approach that of bulk cesium.

THERMAL DESORPTION

Fairly complete measurements have been made by FEPM techniques of the dependence of the heat of desorption on degree of coverage for cesium on a substrate consisting of a clean single-crystal tungsten tip. Such a substrate exposes a variety of crystal planes, and, with one exception to be discussed, the values obtained are effective averages over these various planes.

Thermal Desorption of Atomic Cesium

The basic data are shown in the curve of figure 2 for the measured work function following heating for 60 seconds at successively high temperatures for a tip with a high initial cesium coverage. Langmuir's $\varphi(\theta)$ data (fig. 3) can be used to associate specific degrees of coverage to the data points to the right of point B in figure 2, so that the reduction in coverage $\Delta\theta$ caused by each 60-second heating period can readily be determined. The average heat of desorption E_a associated with a small coverage interval (θ to $\theta - \Delta\theta$) is easily determined by substituting $\Delta\theta$ and $\Delta t = 60$ seconds for $d\theta$ and dt in the relation, according to first-order reaction rate theory (ref. 14),

$$-\frac{d\theta}{dt} = k_a\theta \tag{4}$$

where k_a is a rate constant given by

$$k_a = \nu \exp\left[-\frac{E_a}{RT}\right] \tag{5}$$

A suitable value must be assumed for the vibration frequency ν. The results shown in curve 1 of figure 4 assume $\nu = 10^{11}$ seconds^{-1}. The correctness of this assumption was checked and confirmed, in the coverage range $\theta = 0.22$ to 0.15, by using the rigorous but time-consuming method of determining the time required to change the coverage from $\theta = 0.22$ to 0.15 monolayer at several temperatures and then deriving E_a from the slope of the corresponding plot of t against $1/T$, which is shown by curve 5 of figure 5 and yields $E_a = 48 \pm 2$ kilocalories per mole.

In the present case where the coverage intervals $\Delta\theta$ are not infinitely small, it can be shown that the average heat obtained by the foregoing method is strongly weighted toward the maximum value encountered during the interval, that is, toward the value E_a at final coverage where θ decreases (through desorption) and where $dE_a/d\theta < 0$; curve 1 in figure 4 has been traced accordingly. The lowest heat (18 kcal/mole for $0.67 < \theta < 1$) was obtained by assuming $\theta = 1$ at point B of figure 2 for reasons given earlier. There is some evidence that the observed vibrational frequency decreases with decreasing heat of desorption (ref. 15); if this occurs in the present case, the heat of desorption at $\theta = 1$ would be somewhat lower than is indicated in figure 4.

For comparison purposes, Langmuir's data (ref. 2) for $E_a(\theta)$ are reproduced as curve 2 of figure 4. The results of the investigation herein differ significantly, particularly at high θ; however, the heat of desorption would be expected to approach the heat of sublimation of cesium at high θ (i.e., 18 kcal/mole (ref. 16)), which leads to the belief that the values of this investigation are more nearly correct. This marked difference in heat of desorption is of practical significance because it strongly affects evaporation rates, lower values at high θ leading to higher evaporation rates at a given temperature, and therefore to a lower equilibrium coverage for a given rate of supply from the vapor phase, particularly at moderately low substrate temperatures for which the equilibrium coverage is fairly high.

An interesting consequence of the anisotropy of the substrate is the marked change, shown in figure 6, which occurs in the relative emission from different substrate crystallographic planes as the temperature is raised. Whereas the {110} and the {211} planes have the highest work functions (6.0 and 4.8 ev, respectively) and therefore the lowest emission for clean tungsten (fig. 6(i)), they become the most strongly emitting in the temperature range 300° to 700° K (figs. 6(e) and (f)). In the range 700° to 900° K, emission becomes essentially confined to the vicinity of the {110} planes. It may be noted that this reversal of the emission pattern demonstrated here in high vacuum and over a wide range of temperatures by pulsed FEPM techniques has also been observed in a dynamic system and at high temperatures using thermionic-emission-projection microscopy (ref. 5).

This reversal may be accounted for by the expected dependence on substrate crystal orientation of two quantities: the rate of change $d\varphi/d\theta$ of work function with degree of coverage, particularly at low coverages, and the heat of desorption of cesium. At least at low degrees of coverage, the net dipole per adsorbed cesium atom should be larger on high-work-function substrate planes, causing a larger reduction of the work function of these planes even if a uniform coverage is assumed. Furthermore, such high-work-function planes may also corre-

spond to a larger binding energy for cesium (see following section) and thus to lower evaporation rates for adsorbed cesium, leading to a relatively higher cesium coverage on these planes at substrate temperatures sufficient to cause appreciable cesium evaporation. Both of these factors probably contribute to the observed effect.

Ionic and Atomic Desorption at Low Cesium Coverage

The foregoing derivation of the heat of desorption $E_a(\theta)$ for atomic cesium is valid only if the observed decrease in degree of coverage is caused by desorption in atomic rather than ionic form. This is certainly the case above $\theta = 0.10$ (at least in the absence of strong applied electric fields), since the heat of desorption for ions $E_p(\theta)$, shown by curve 4 of figure 4, which reproduces Langmuir's data (ref. 2), is larger than $E_a(\theta)$ for $\theta < 0.10$. To determine the heat of desorption for atomic cesium at coverages below the crossover of the $E_p(\theta)$ and $E_a(\theta)$, the FEPM was operated with a positive d-c bias voltage applied to the screen, to return desorbed ions to the tip and of sufficient magnitude to limit desorbed ions having thermal energy to excursions outside the tip surface of less than one lattice parameter, so that desorbed ions would in all probability be returned to their initial adsorption site. In this manner, terminal desorption over the range $\theta = 0$ to 0.07 was investigated for two different screen bias voltages (650 and 1500 v, corresponding to field strengths at the tip of 6 and 13 Mv/cm) to allow the estimate of the field effect on $E_a(\theta)$ required for comparison of this data with the zero-field values obtained at higher degrees of coverages. These measurements led to the two Arrhenius plots shown by curves 1 and 2 of figure 5.

Two facts emerge from these results. First, there is no marked variation of $E_a(\theta,F)$ over a twofold variation in applied field strength. This is not unexpected, since the field dependence of the heat of desorption for atomic cesium is the sum of two terms, $1/2\ \alpha F^2$ and μF, where α is the polarizability and μ is the permanent dipole moment, both of which are relatively small at the field strengths used herein. Thus, the values obtained (67±2 and 69±2 kcal/mole) also represent the zero-field heat of desorption of atomic cesium at $\theta = 0$. Second, the measured heat of atomic desorption varies very rapidly with degree of coverage as θ approaches zero, even more rapidly than found by Langmuir, and the terminal value at $\theta = 0$ (68±2 kcal/mole) is in close agreement with the value obtained by Langmuir (69 kcal/mole).

The heat of ionic desorption $E_p(\theta)$ is theoretically related to the heat of atomic desorption $E_a(\theta)$, in the absence of applied field, by the expression

$$E_p(\theta) = E_a(\theta) + V_I - \varphi(\theta) \qquad (6)$$

where $V_I = 3.87$ electron volts is the ionization potential of cesium. Curve 3 of figure 4 shows the $E_p(\theta)$ curve derived in this manner from Langmuir's $\varphi(\theta)$ data (fig. 3) and the $E_a(\theta)$ data of this investigation (curve 1 of fig. 4). It is interesting to note that this calculated curve for $E_p(\theta)$, based on $E_a(\theta)$ data for a single tungsten crystal, exhibits a minimum at $\theta = 0.02$, a phenomenon observed experimentally by Langmuir for polycrystalline surfaces. This calculated minimum is a direct consequence of the very steep decrease of $E_a(\theta)$ with

increasing θ near $\theta = 0$, which is sufficient to override the decrease of $\varphi(\theta)$ so that, in view of equation (4), $dE_p(\theta)/d\theta < 0$ near $\theta = 0$.

As a direct experimental check of the values so calculated for $E_p(\theta)$ near $\theta = 0$, the terminal desorption experiment was repeated over the same range of coverages ($\theta = 0$ to 0.07) but with either no d-c bias voltage or a small negative bias voltage at the screen, so that desorption in ionic form is permitted. As compared with the previous case of atomic desorption, the corresponding Arrhenius plots (curves 3 and 4 of fig. 5) are shifted to lower temperatures and yield a lower value of the heat of desorption, that is, 55±2 kilocalories per mole in both cases. In view of the foregoing discussion, this value represents the maximum heat of desorption of cesium ions over the range $\theta = 0$ to 0.07 and is indeed found to agree very closely with the $E_p(\theta)$ values derived from the $E_a(\theta)$ data of this investigation by means of equation (6).

Finally, an analysis of the sequence of field-emission patterns obtained during the terminal desorption phase confirms the features indicated previously for the $E_a(\theta)$ and $E_p(\theta)$ curves near $\theta = 0$ and suggests an explanation of these features based on the anisotropy of the crystalline substrate. The need for an explanation is apparent since Langmuir explained the steep slope of the $E_a(\theta)$ curve near $\theta = 0$ and the minimum in the $E_p(\theta)$ curve by assuming the simultaneous existence of two surface phases, where the second phase is associated with crystal boundaries (ref. 2). However, the data herein indicate an increase in the slope of the $E_a(\theta)$ curve near $\theta = 0$, which is even more pronounced than that observed by Langmuir and which cannot be explained by Langmuir's hypothesis, since the measurements of this investigation were made on a single-crystal tip that contained no grain boundary.

Figure 7 shows a representative sequence of field-emission pattern photographs taken at a fixed screen voltage during the terminal desorption phase. The same sequence is found in all cases (zero, negative, or positive d-c bias voltage applied at the screen); however, the fraction of the total desorption time necessary to proceed from the patterns in figures 7(c) to (d) was much greater with a positive bias (which prevents ionic desorption) than in the other two cases where ionic desorption predominates, thus confirming that, as θ decreases from 0.07 to 0, the heat of atomic desorption increases much more rapidly than the heat of ionic desorption. Also, comparison of patterns in figures 7(b), (c), and (d) shows steady darkening of the {110} regions (therefore, steady increase in φ and steady decrease in θ for these regions) but shows little or no change in other regions, indicating that cesium coverage of these other regions was essentially constant. Since the final pattern corresponds to complete removal of the adsorbed cesium, it may be concluded that these other regions were essentially free of cesium as early as the pattern shown in figure 7(b), so the heat of desorption measured for the final stage of desorption should be associated with the {110} crystal planes of the substrate. In opposition, examination of patterns in figures 6(d) ($\theta = 0.67$) to (g) ($\theta = 0.2$) indicates that the more pronounced changes in emission, and therefore in θ, occur in regions other than the {110}. Therefore, $E_a(\theta)$ values obtained at $\theta > 0.2$ are associated with these regions rather than with {110} planes. Thus, Langmuir's observation that the existence of more than one state of binding for adsorbed cesium can account for the observed behavior of the $E_a(\theta)$ and $E_p(\theta)$ curves near $\theta = 0$ appears correct, but at least in the experiments of this investigation the existence of several states

of binding simply appears to be a direct consequence of the anisotropy of the crystalline substrate. A different binding energy would be expected for each crystallographic orientation of the substrate; however, as indicated by other properties (e.g., surface tension, work function), the anisotropy of tungsten is not pronounced except for the {110} planes, which differ markedly from other crystal orientations.

In view of the data herein, it is suggested that this marked differentiation also occurs for cesium adsorption, the {110} regions being characterized by substantially higher binding energy for adsorbed atomic cesium. On this basis, the sharp increase observed in $E_a(\theta)$ below $\theta \cong 0.2$ would be expected to occur when θ becomes sufficiently low so that a large and increasing fraction of the residual cesium is concentrated on {110} planes and desorption from such planes becomes predominant over that from other regions of the substrate. This observed concentration of cesium at a low degree of coverage on the high-work-function {110} planes clearly shown by the results of this investigation is of course of distinct interest and advantage for contact-ionization work.

SURFACE MIGRATION AT LOW TEMPERATURES

The methods being used herein provide a sensitive technique for the detection of very slow migration because of the high magnification and small emitter size of the FEPM. It was found that cesium deposited on tungsten begins to diffuse at temperatures well below room temperature by one of two different modes of surface diffusion, the predominating mode depending on the amount of initial cesium dose.

High Initial Coverage

In the absence of an applied field and for high initial cesium coverage, migration is readily observed at substrate temperatures down to 170° K. Figure 8 shows a typical sequence of field-emission patterns taken at 187° K; as the migration proceeded, the pulsed screen voltage was adjusted to maintain an approximately constant pulsed-field-emitted current. Figure 8(a), taken at 77° K after the tungsten emitter had been heated to 2400° K to provide a clean and smooth surface, shows a pattern characterisitic of clean tungsten. Figure 8(b) identifies the major crystal planes for the tungsten crystal orientation of figure 8(a). Figure 8(c) shows the pattern after an estimated 1.6 monolayers of cesium had been evaporated onto one side of the tip held at 77° K. Emission occurred only from the cesium-covered portion because of the much lower work function of that region. Figures 8(d) to (i) are successive patterns obtained after raising the temperature to 187° K. The migration of the cesium over the tungsten substrate is shown, and the following conclusions are suggested:

(1) In figure 8, the boundary of the cesium-covered region remains quite sharp as it progresses (at the rate of approx. 2×10^{-7} cm/sec at 187° K). This behavior, typical of high degrees of initial coverage, suggests that in such cases cesium spreads primarily as a result of relatively mobile "second-layer" cesium atoms migrating over the edge of the more tightly bound first atom layer in direct contact with the cesium substrate.

(2) The activation energy E_d in kilocalories per mole for this mode of diffusion can be calculated from

$$E_d = 4.6 \times 10^{-3} \, T \log\left(\frac{t\nu a^2}{x^2}\right) \tag{7}$$

where t is the time for the sharp boundary to move a distance x between easily identifiable planes of the pattern at a temperature T, a is the distance between adjacent adsorption sites, and ν is the vibrational frequency of the adsorbed cesium atoms. Using $t = 170$ seconds, $x = 3000$ angstroms, $T = 187^\circ$ K, $a = 3$ angstroms, $\nu = 10^{11}$ seconds^{-1}, an activation energy of approximately 6.2 kilocalories per mole (0.27 ev) is obtained, which is in fair agreement with Langmuir's estimate of 0.2 electron volt for diffusion in the second layer (ref. 2).

(3) The boundary proceeds nonuniformly, indicating the migration of second-layer cesium atoms is influenced to some extent by the crystal structure of the tungsten substrate.

Low Initial Coverage

A second mode of diffusion, illustrated in the field-emission patterns of figure 9, is observed when the initial dose is appreciably less than 1.0 monolayer. The final degree of coverage in figure 9 is 0.12 monolayer, as determined from the work function measured after completion of the migration process. From this it is inferred that the average initial coverage was at least 0.24 monolayer. If desorption accompanies surface migration, the initial coverage calculated this way will be correspondingly higher; however, as was shown earlier, the desorption energies in the coverage range in which these migration studies were performed are considerably higher than migration energies. It should be pointed out that this justification is valid only if migration is measured over essentially the same collection of sites that the desorption energies are referred to, if the latter varies appreciably with coverage. The desorption energies from the (110) plane and vicinity are sufficiently high compared with the corresponding migration energies that desorption is negligible during migration over this region. In the case of the (100) region and its nearby higher index planes, migration energies are found to be somewhat higher and may approach desorption energies from these planes, which, although not directly measurable by the technique used herein, give indication of being quite low. It is thought this latter condition may account for the lack of sharp boundary diffusion over the (100) region and the apparent small concentration of cesium in this region, as shown in figures 9(e) and 10(d).

To determine the effect of the atomic surface structure of the substrate, reference patterns (figs. 9(b), (c), (d), and (e)) were selected such that the transition from one pattern to the next corresponded to cesium migration over fairly well defined substrate crystal planes. Transition A corresponds primarily to migration over smooth close-packed (110) ledges, transition B corresponds to migration over the edges of such (110) ledges, and transition C corresponds to migration over the rougher areas (on an atomic scale) in the (100) region.

Measurement of the temperature dependence of the times required for each transition led to the Arrhenius plots of figure 11(a). From the slopes of the straight lines corresponding to each transition are derived their corresponding activation energies of 11.0±0.5, 12.3±0.5, and 17.4±0.5 kilocalories per mole for transitions A, B, and C, respectively. (The probable errors simply represent the observed scatter in the data.) These activation energies are in the order expected from a consideration of the degree of atomic structure and roughness of the substrate surfaces involved in each transition and bracket the average value of 14 kilocalories per mole obtained by Langmuir for a polycrystalline surface (ref. 1).

A preliminary investigation of the effect of degree of coverage on this mode of surface diffusion has been made. At a higher initial dose of 0.66 monolayer (inferred from a final uniform coverage of 0.33 monolayer), the activation energies for the three transitions were found to be approximately the same. However, as can be seen in the emission patterns of figure 10, the actual amount of cesium diffusing across the emitter surface may be approximately the same as in figure 9 even though the initial dose was larger. When the initial dose exceeds 0.5 monolayer, an additional receding boundary is observed indicating the onset of certain cohesive forces between adsorbed cesium atoms. It would appear that the original dose supplies just enough cesium to maintain the diffusion (the dose "cap" shrinks as the leading edge of the diffusing cesium progresses), in which case the activation energies for migration would be expected to be insensitive to initial coverage. The latter is strictly correct only if site-to-site migration in the advancing cesium boundary is the rate-determining step and not the process of cesium migration out of the high concentration region. Qualitatively, it appears that the advancing and receding boundaries move at nearly equal rates and probably with similar activation energies. The origin of the cohesive forces responsible for condensation into this higher concentration phase is not presently well understood, since repulsive forces between adsorbed dipoles are normally assumed to predominate. At a lower degree of coverage (0.08 monolayer initial, 0.04 monolayer final) lower activation energies are obtained (from fig. 11(b), 8.3±0.5 kcal/mole for transition A and 9.6±0.5 for transition B, not measured for transition C). In this case (fig. 12), the amount of cesium migrating across the surface is definitely less than that for the transitions shown in figure 9, as evidenced by the reduced contrast between the brightness of the cesium-covered and noncovered regions of the pattern.

In general, the results herein agree with Langmuir's earlier value and, in addition, provide a confirmation and a measurement of the variation of the surface migration rates and activation energies with the crystal orientation of the tungsten substrate. This variation, in turn, implies the existence of strong local variations in equilibrium degree of coverage for substrate surfaces, which expose a variety of crystal planes (e.g., polycrystalline surfaces) at least for substrate temperatures near room temperature.

EFFECT OF EXTERNALLY APPLIED ELECTRIC FIELD ON SURFACE MIGRATION

Despite the existence of the field-emission microscope for some time and its wide application to surface-diffusion studies, very little quantitative data regarding field effects of surface diffusion are currently available. It has been

reported in reference 17 with the use of nonfield-emission techniques that the diffusion coefficient D for surface diffusion of cesium on tungsten at 1500° K decreases with increasing positive fields from 5 to 25 kilovolts per centimeter. The current study of the same system with the use of field-emission techniques allows the extension of applied fields of either polarity to 20 megavolts per centimeter and, in addition, the ability to examine the field effect of surface diffusion on a particular crystallographic plane.

Measurements of the activation energy of surface diffusion E_d as a function of applied field were accomplished in a manner analogous to the zero-field experiments. The maximum positive field strength under which surface diffusion rates are measurable is limited by the onset of field desorption, which becomes appreciable at fields greater than 20 megavolts per centimeter. Excessive field emission, on the other hand, limits negative fields to approximately the same field strength.

Experimental Results

The field dependency of the activation energy of surface migration was measured over the diffusion modes indicated in transitions A and B in figure 9. The end-point field-emission patterns used in measuring the rates of these diffusion modes were not altered visually by the application of the field. However, at high positive and negative fields, the diffusion mode in transition A seemed to proceed more rapidly relative to the mode in transition B.

The temperature dependency of the diffusion rates in the presence of an electric field was found to obey the Arrhenius equation, thus permitting the calculation of activation energies E_d of surface diffusion, which are listed in table I. It is therefore assumed that the diffusion coefficient D obeys the relation

$$D = \frac{x^2}{t} = p\nu a^2 \exp\left[-\frac{E_d}{kT}\right] \tag{8}$$

where p is the probability of a successful site change per vibration. For convenience, the pre-exponential factor $pa^2\nu$, in which p and ν are constant, will be referred to as A and is also listed in table I. The distance x can be obtained from elementary geometrical consideration provided that the tip radius and angular change of the migrating cesium boundary are known. The angular change can be determined from the field-emission patterns by using the known angular separation of appropriate crystal planes, while the tip radius can be estimated from clean tip Fowler-Nordheim plots. The tip radius pertaining to the current study was estimated at 2500±500 angstroms.

Diffusion coefficients calculated at 200° and 1000° K are shown in table I as D/x^2, where x is approximately 1500 angstroms for both A and B type migration. At high temperatures, the results of this report agree in trend with those of reference 17. It should be pointed out, however, that these diffusion coefficients measured in the temperature range from 150° to 200° K can be extrapolated to 1000° K only if E_d and A remain temperature independent at high temperatures.

The results shown in table I indicate a decrease in diffusion energy E_d with either positive or negative fields at the tip, although the effect is more pronounced with positive fields. It is also noted that a significant decrease in the pre-exponential factor A occurs with increasing field. Again, the effect is also more pronounced at positive fields. A similar field dependency of both A and E_d has been reported for barium on tungsten (ref. 15).

Theoretical Model

The potential energy of an adsorbed atom migrating over various atomically smooth crystallographic planes is generally regarded to imitate, to some extent, the physical surface; thus, a saddle and trough potential surface is expected to apply to a migrating adsorbed atom, as depicted in figure 13. The height of the barriers, which determines the activation energy for diffusion, is known to vary with adsorbate, crystallographic plane, direction of migration, adsorbate concentration, and applied field.

An expression relating variations of E_d with applied field F can be obtained from classical electrostatic considerations by using a modified version of the model described in reference 18. According to these considerations the effect of an external electric field is to induce a dipole in an atom migrating on the surface, which results in an additional binding energy E_b given by

$$-E_b = \frac{1}{2}\alpha F^2 \pm \mu F \tag{9}$$

where α is the polarizability and μ the dipole moment of the migrating atom. The second term of equation (9) depends on the sign of the field relative to μ and is due to the interaction of field with the permanent dipole moment of the adsorbed atom.

If the atomic structure of the surface is considered, the field at the surface may be represented, as illustrated in figure 13, where F_p is defined as the average field corresponding to an ideally smooth surface with a field enhancement factor k of unity, $F_t = k_t F_p$ is the field at the trough position $k_t < 1$, and $F_s = k_s F_p$ is the field at the saddle position that the atom must cross when migrating from one site to the next $k_s > k_t$. It follows that the activation energy E_f for surface migration in an applied field will decrease with field according to the expression

$$E_f = E_d - \frac{1}{2}\alpha F_p^2(k_s^2 - k_t^2) \pm \mu F_p(k_s - k_t) \tag{10}$$

where E_d is the activation energy of migration with no applied field, and the third term is positive when the screen voltage is positive relative to the tip, or, alternatively, when μ and F are in the same direction.

Comparison of Theory and Results

The results shown in table I are plotted in figure 14 according to equa-

tion (10) written in the form

$$E_f = E_d \pm BF - CF^2 \tag{11}$$

The points at the highest positive field (F = 13.3 Mv/cm) may be somewhat unreliable because of the possibility of simultaneous field desorption. A closer fit of the data to equation (11) is obtained if these high field points are omitted. A similar deviation at high positive fields was reported for barium diffusion on tungsten (ref. 15) and attributed to a field-induced electronic transition to the ionic state while crossing the saddle point of the potential energy diagram.

A least-squares analysis of the data gives a reasonable fit (rms deviation ±0.5 kcal/mole) with E_d = 9.96, B = 0.16, C = 0.0079 for transition A and E_d = 11.5, B = 0.22, C = 0.019 for transition B migration (solid lines in fig. 15).

The larger value of the coefficients B and C for transition B migration probably reflects a greater difference between k_s and k_t, which would be expected if diffusion over (110) lattice steps is rate-determining for this mode. The difference $k_s - k_t$ will be influenced both by substrate geometry and adsorbate size. For example, a greater shielding of the field is expected for smaller adsorbates that can fit deeper into the lattice sites when in the trough position, thus leading to a smaller k_t or a greater $k_s - k_t$. A loose-packed substrate surface, by similar arguments, should yield a larger $k_s - k_t$ than a close-packed surface. It should be emphasized that an increasing value of $k_s - k_t$ with decreasing adsorbate size does not necessarily lead to a larger field effect, since C (the coefficient of the F^2 term) also involves the polarizability, which normally decreases with decreasing adsorbate size.

A further consequence of equation (11) is the maximum in E_f that occurs at a field strength of

$$F_{max} = \pm \frac{B}{2C} \tag{12}$$

The value of F_{max} is negative for the present study involving electropositive adsorbates; this follows from the fact that B contains μ, which determines the sign of equation (12). The results herein for an electropositive adsorbate, namely cesium, substantiate equation (12) and give a value of F_{max} = 8 megavolts per centimeter for both type A and type B migration.

The known values of the coefficients B and C of equation (11) involve μ, α, k_t, and k_s and do not allow an explicit determination of all four unknowns. Substituting these unknowns for B and C in equation (12), the following relation can be obtained:

$$F_{max} = \frac{\mu}{\alpha(k_s + k_t)} \tag{13}$$

Estimates of the polarizability of adsorbed cesium were made according to equation (13), whereby the expression for α becomes, for type A,

$$\alpha = \frac{166}{k_s + k_t} \times 10^{-24} \text{ cm}^3 \tag{14}$$

and, for type B,

$$\alpha = \frac{281}{k_s + k_t} \times 10^{-24} \text{ cm}^3 \tag{15}$$

using the data of this report for F_{max} and $\mu = 5.5 \times 10^{-18}$ esu from reference 19. It is doubtful from referring to the original model depicted in figure 13, that $k_s + k_t$ can exceed 3 or 4, thus giving calculated values of α in the range of the known atomic polarizabilities, which vary from 40 to 60×10^{-24} cubic centimeter (refs. 20 and 21). This indicates the adsorbed state to exist as a polarized atomic state rather than an ionic state, since the measured polarizability of singly charged cesium, reported to be 3.3×10^{-24} cubic centimeter (ref. 22), is an order of magnitude lower than the atomic state polarizabilities.

The explanation of the pronounced variation of the pre-exponential A with applied field, as shown in figure 14, is not obvious at this time. It is speculated to arise through variations of the factors due to field-induced electronic transitions involved in the diffusion process or entropy effects. One important consequence of the strong field dependency of A is shown by the difference between the curves of figures 15 and 16, where it is observed that at higher temperatures the variation of D with field is determined by A instead of E_d.

CONCLUDING REMARKS

These studies have shown that, at degrees of coverage approaching 1.0 monolayer, measurable thermal desorption of cesium atoms occurs down to room temperature and corresponds to an activation energy substantially lower than that previously quoted by Taylor and Langmuir; however, for nearly clean tungsten in high vacuum the temperatures required to remove the last 0.05 monolayer within approximately 10 seconds are 870° and 1000° K for desorption in the form of ions and neutral atoms, respectively. Field-emission patterns indicate that the cesium atoms are most tightly bound, with respect to both ionic and neutral desorption, to the high-work-function crystal planes of the substrate, and particularly the (110) planes for tungsten.

Surface diffusion of cesium on tungsten has been observed to occur at temperatures as low as 170° K and is quite rapid at room temperature. (From the experimental results of this investigation the diffusion may be calculated to be $D = 10^{-8}$ square centimeter per second at 300° K for 0.24 monolayer initial coverage on the (110) plane.) Whereas a dependence of the surface diffusion activation energy on substrate crystallographic direction exists, the dependence is not as large as that observed for many other adsorbates, indicating that the relatively large diameter of cesium atoms has the effect of diminishing the influence of substrate atomic structure on diffusion.

Surface diffusion rates are found to depend on both the magnitude and the polarity of a d-c electric field applied at the surface. If the surface diffu-

sion coefficient D is expressed in the usual Arrhenius form

$$D = A \exp\left[-\frac{E_d}{kT}\right]$$

it is found that, over the range of applied field which was investigated (i.e., from -22 to 13 Mv/cm), the expected decrease of the activation energy E_d with increasing applied field is accompanied by a decrease in the pre-exponential factor A, which has an opposite effect on the diffusion coefficient D. At temperatures above 300° K, the changes in pre-exponential factor A predominate and, as shown in figure 16, the diffusion coefficient D is largest for zero field and is reduced by an applied field of either polarity. Whereas the observed field dependence of A is not predicted by the simple physical model for diffusion and is not yet fully understood, it is found that the observed field dependence of E_d agrees with that predicted on the basis of a model consisting of both field-permanent-dipole and field-induced-dipole interactions, when suitable values are assumed for the permanent dipole moment and the induced polarizability. In turn, the polarizability of adsorbed cesium, which is derived from the $E_d(F)$ data in this manner, is quite high and therefore suggests that the adsorbed state of cesium on tungsten is atomic rather than ionic, at least at the degree of coverage $\theta = 0.24$ used in this particular experiment.

In the course of the foregoing experiments, thin cesium layers (up to 1.0 monolayer) adsorbed on a tungsten substrate have been observed under conditions involving substrate temperatures from 77° to about 1000° K, and applied electric fields up to 3×10^7 volts per centimeter in the direction favoring field emission and up to 5×10^7 volts per centimeter (for a monolayer at 77° K) in the direction favoring desorption of ions. Under such conditions, the cesium layers have remained fairly smooth and "well-behaved;" that is, they have exhibited no tendency to build up crystallites or projections that would enhance the probability of voltage breakdown across a vacuum gap between cesium-coated electrodes. These observations indicate that the breakdown strength of vacuum gaps between cesium-coated electrodes is, in fact, quite high and suggest that other phenomena have been largely responsible for difficulties often encountered in cesium systems.

Lewis Research Center
National Aeronautics and Space Administration
Cleveland, Ohio, 9/13/63

APPENDIX - SYMBOLS

A	pre-exponential factor in diffusion equation (eq. (8)), cm/sec^2
A'	intercept of Fowler-Nordheim plot (eq. (1)), amp/v^2
a	distance between adjacent adsorption sites on atomic surface, A
B,C,E_o	arbitrary constants in quadratic expression (eq. (11))
D	diffusion coefficient, cm/sec^2
E_a	heat of atomic desorption, kcal/mole
E_b	change in binding energy due to field-dipole and dipole-dipole interactions (eq. (9)), kcal/mole
E_d	activation energy for surface migration, kcal/mole
E_f	activation energy for field-dependent surface migration, kcal/mole
E_p	heat of ionic desorption, kcal/mole
F	surface electric field, Mv/cm
F_p,F_s,F_t	surface electric field for ideally smooth surface, saddle position on an atomic surface, and trough position, respectively (fig. 14), Mv/cm
I	field-emission current, amp
k_a	rate constant for desorption (eq. (5)), sec^{-1}
k_s,k_t	ratio of F_s and F_t, respectively, to F_p
m	slope of Fowler-Nordheim plot (eq. (1)), v
p	probability of successful site change per vibration
R	universal gas constant, 1.98×10^{-3} kcal/(mole)(^oK)
T	emitter surface temperature, ^oK
t	desorption or diffusion time, sec
V	applied voltage, v
V_I	ionization potential of adsorbate, ev
x	distance that boundary of cesium layer moves across emitter surface, A
α	atomic polarizability, cm^3

β geometric ratio of surface electric field at emitter surface to applied voltage, cm^{-1}

μ dipole moment of adsorbed atom, (coulomb)(m)

ν vibrational frequency of adsorbed atoms, sec^{-1}

θ degree of adsorbate coverage (monolayer)

θ_i initial degree of adsorbate coverage (monolayer)

φ_{av} average work function of emitter surface, ev

Subscripts:

1 clean, uncoated emitting surface

2 coated surface

REFERENCES

1. Langmuir, Irving, and Taylor, John Bradshaw: The Mobility of Cesium Atoms Adsorbed on Tungsten. Phys. Rev., vol. 40, no. 3, Apr. 1932, pp. 463-464.

2. Taylor, John Bradshaw, and Langmuir, Irving: The Evaporation of Atoms, Ions, and Electrons from Caesium Films on Tungsten. Phys. Rev., vol. 44, no. 6, Sept. 1933, pp. 423-458.

3. Johnson, R. P., and Shockley, W.: An Electron Microscope for Filaments: Emission and Adsorption by Tungsten Single Crystals. Phys. Rev., vol. 49, Mar. 1936, pp. 436-440.

4. Martin, S. T.: On the Thermionic and Adsorptive Properties of the Surfaces of a Tungsten Single Crystal. Phys. Rev., vol. 56, no. 9, Nov. 1939, pp. 947-959.

5. Webster, H. F.: Thermionic Emission from a Tantalum Crystal in Cesium or Rubidium Vapor. Sci. Rep. 6, Air Force Cambridge Res. Lab., 1961.

6. Dyke, W. P., and Barbour, J. P.: Pulsed T-F Emission Electron Projection Microscopy. Jour. Appl. Phys., vol. 27, no. 4, Apr. 1956, pp. 356-360.

7. Haefer, R.: Experimentelle Untersuchungen zur Prüfung der wellenmechanischen Theorie der Feldelektronenemission. Zs. Physik, bd. 116, heft 9-10, 1940, pp. 604-623.

8. Müller, Erwin W.: Elektronenmikroskopische Beobachtungen von Feldkathoden. Zs. Physik, bd. 106, heft 9-10, 1937, pp. 541-550.

9. Good, R. H., Jr., and Müller, Erwin W.: Field Emission. Handbuch der Physik, vol. 21, Springer Verlag (Berlin), 1956, pp. 176-231.

10. Dyke, W. P., and Dolan, W. W.: Field Emission. Vol. 8 of Advances in Electronics and Electron Phys., Academic Press, Inc., 1956, pp. 90-185.

11. Gomer, R.: Field Emission and Field Ionization. Harvard Univ. Press (Cambridge), 1961.

12. Dyke, W. P., Trolan, J. K., Dolan, W. W., and Barnes, George: The Field Emitter: Fabrication, Electron Microscopy, and Electric Field Calculations. Jour. Appl. Phys., vol. 24, no. 5, May 1953, pp. 570-576.

13. Gomer, R., Wortman, R., and Lundy, R.: Mobility and Adsorption of Hydrogen on Tungsten. Jour. Chem. Phys., vol. 26, no. 5, May 1957, pp. 1147-1164.

14. Frost, Arthur A., and Pearson, Ralph C.: Kinetics and Mechanism, ch. 2. John Wiley & Sons, Inc., 1953.

15. Utsugi, H., and Gomer, R.: Field Desorption of Barium from Tungsten. Jour. Chem. Phys., vol. 37, no. 8, Oct. 1962, pp. 1706-1719.

16. Taylor, John Bradshaw, and Langmuir, Irving: Vapor Pressure of Caesium by the Positive Ion Method. Phys. Rev., vol. 51, no. 9, May 1937, pp. 753-760.

17. Shelton, H.: Surface Diffusion Studies of Cesium on Tungsten. ARS Jour., vol. 32, no. 5, May 1962, pp. 708-710.

18. Drechsler, Michael: Kristallstufen von 1 bis 1000 A. Zs. Elektrochem., bd. 61, no. 1, 1957, pp. 48-55.

19. Moore, George E., and Allison, H. W.: Adsorption of Strontium and of Barium on Tungsten. Jour. Chem. Phys., vol. 23, no. 9, Sept. 1955, pp. 1609-1621.

20. Scheffers, H., and Stark, J.: The Influence of an Electric Field on Alkali Atoms in Atomic-Beam Experiments. Physik. zs., vol. 35, 1934, pp. 625-627.

21. Fues, E.: Bemerkung zur Abschätzung der Polarisierbarkeiten der Neutralen Alkaliatome. Zs. Physik, bd. 82, heft 7-8, 1933, pp. 536-537.

22. Tessman, Jack R., Kahn, A. H., and Shockley, William: Electronic Polarizabilities of Ions in Crystals. Phys. Rev., vol. 92, no. 1, Nov. 1953, pp. 890-895.

TABLE I. - EFFECT OF D-C FIELD ON SURFACE MIGRATION (CESIUM ON TUNGSTEN)

AT INITIAL DEGREE OF ADSORBATE COVERAGE OF 0.24

Type	Surface electric field, F, Mv/cm	Activation energy for surface migration, E_d, kcal/mole	Logarithm of pre-exponential factor, A	Logarithm of diffusion coefficient	
				Log $D_{200^\circ K}/x^2$	Log $D_{1000^\circ K}/x^2$
A	-21.8	9.7	7.6	-2.9	5.5
B	-21.8	7.4	4.6	-3.4	3.0
A	-13.9	10.4	9.0	-2.3	6.7
B	-13.9	11.0	8.7	-3.3	6.3
A	-6.64	10.7	10.0	-1.6	7.7
B	-6.64	12.0	10.4	-2.6	7.8
A	0	11.0	10.4	-1.6	7.5
B	0	12.3	11.3	-1.6	8.6
A	4.45	8.7	8.8	-.7	6.9
B	4.45	9.9	9.8	-1.0	7.6
A	8.8	7.8	8.3	-.2	6.6
B	8.8	7.5	7.5	-.6	5.9
A	13.3	6.6	7.3	.1	5.9
B	13.3	5.7	5.6	-.6	4.4

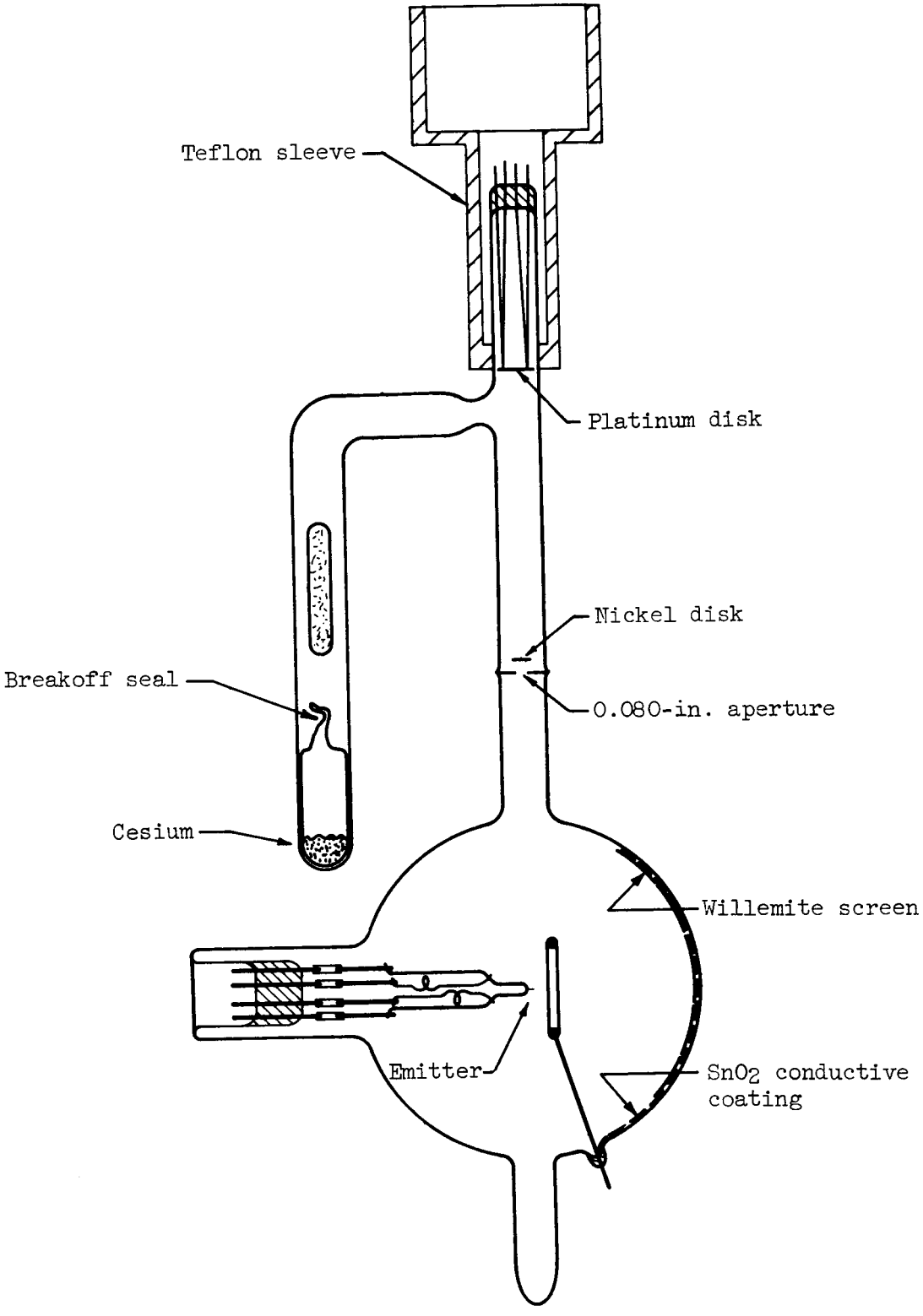

Figure 1. - Diagram of the experimental tube.

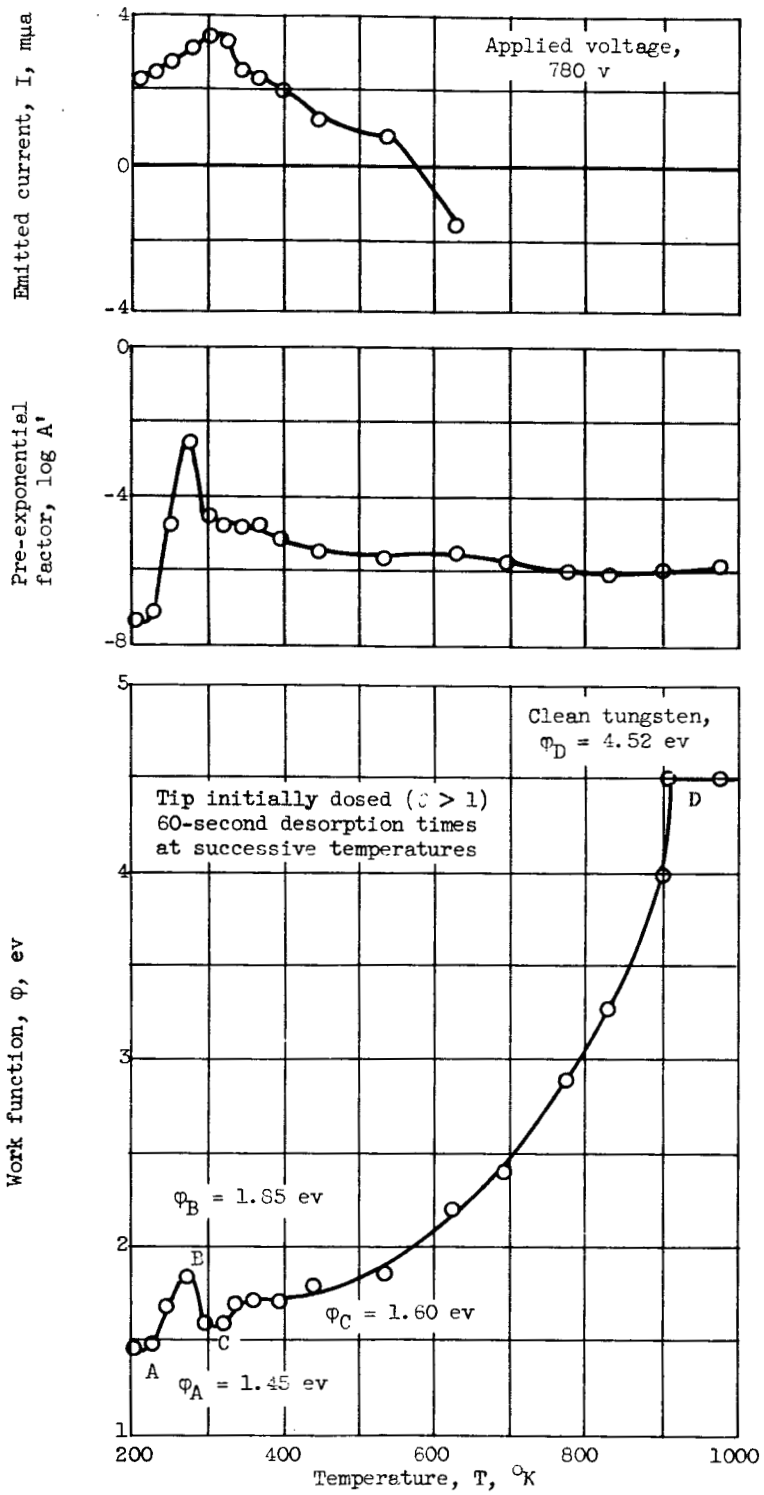

Figure 2. - Field-emitted current at constant voltage, pre-exponential factor A', and work function as functions of temperature to which emitter has been heated successively for 60 seconds.

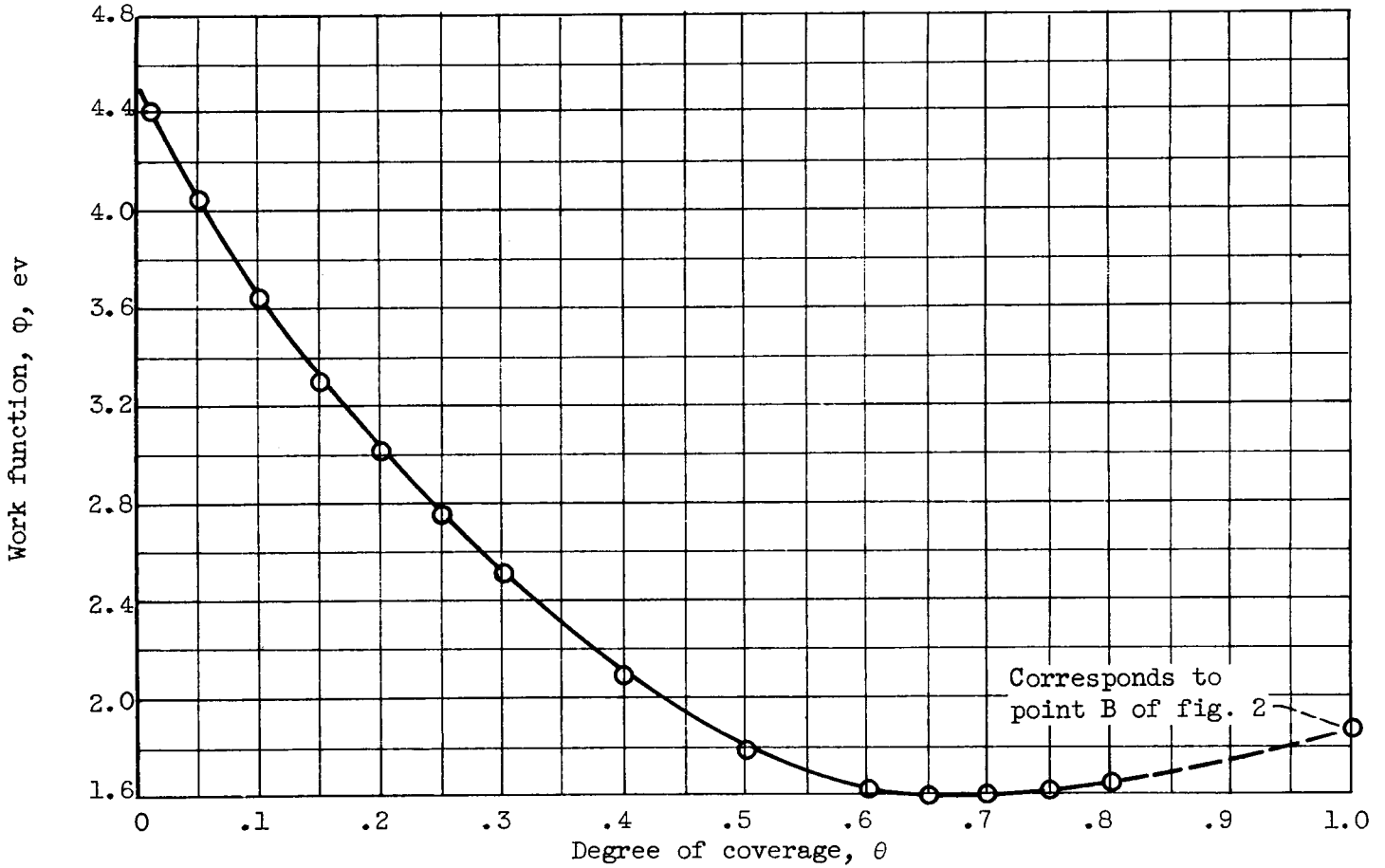

Figure 3. - Work function against degree of coverage from Taylor and Langmuir (ref. 2).

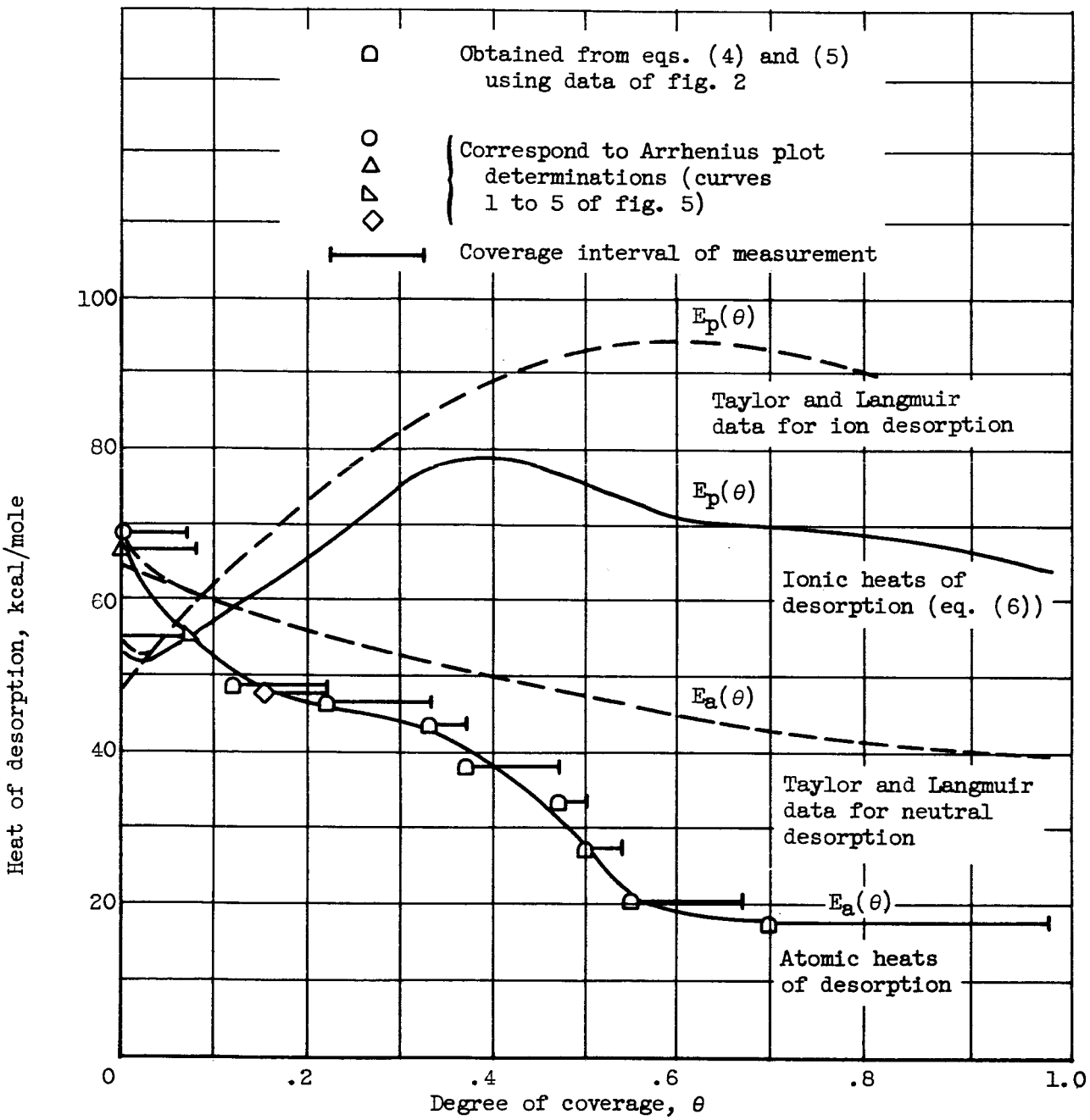

Figure 4. - Heats of desorption at various degrees of coverage.

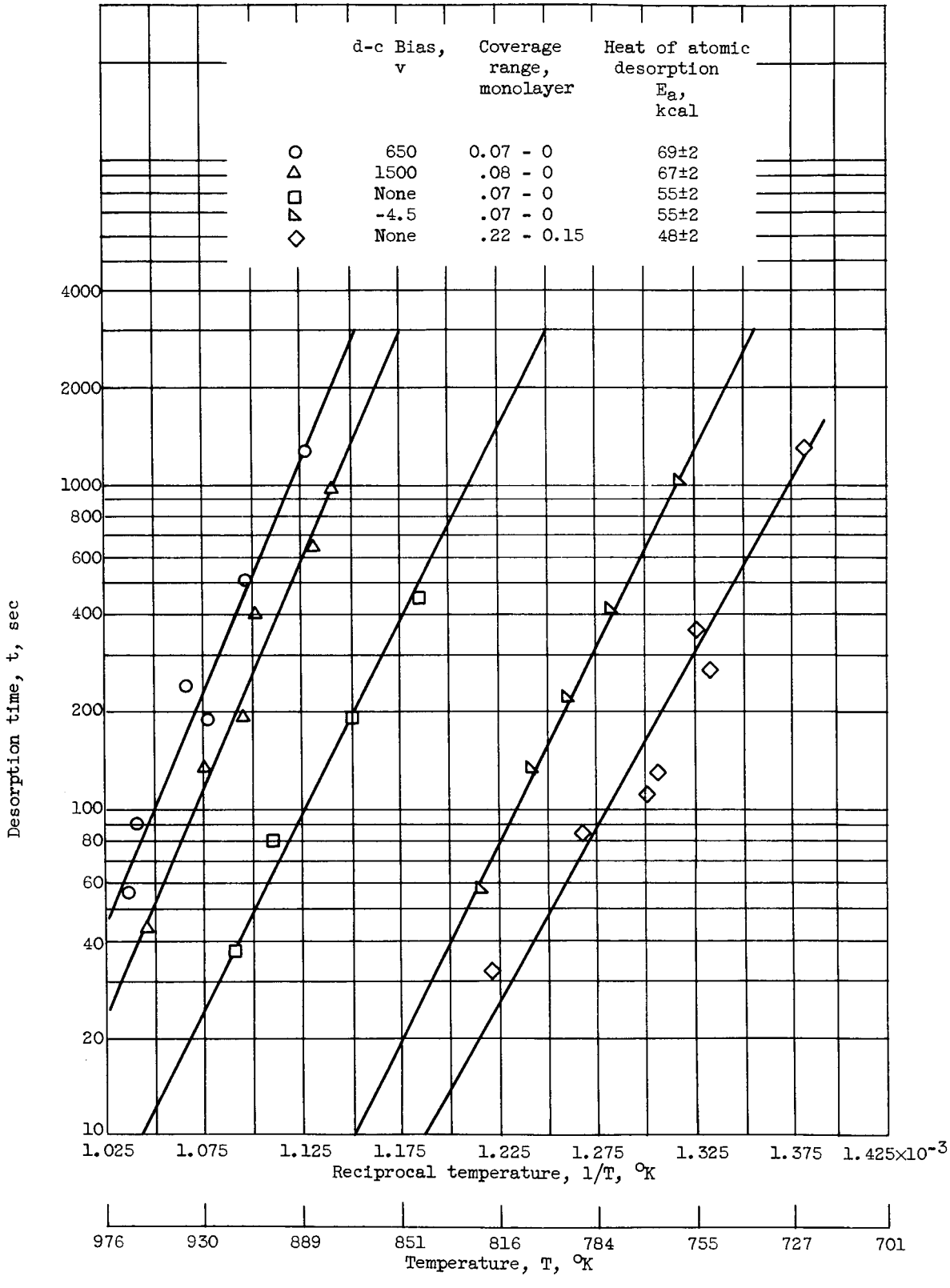

Figure 5. - Arrhenius plots of thermal desorption data.

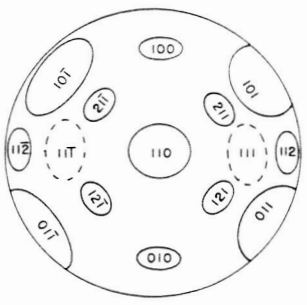

(a)

Diagram of principal planes of body-centered cubic pattern

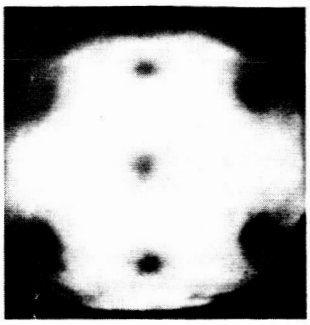

(b)

Emitter surface temperature: 201° K
Work function: 1.45 ev

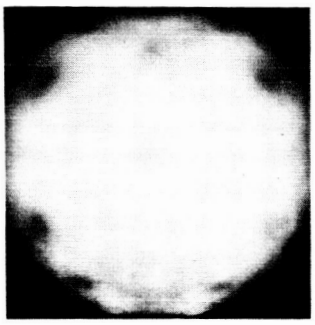

(c)

271° K
1.85 ev

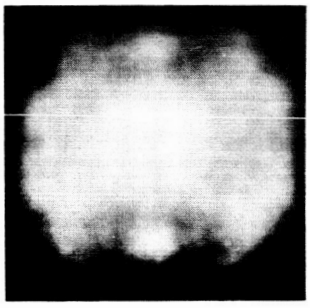

(d)

295° K
1.60 ev

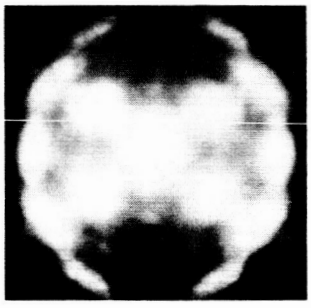

(e)

317° K
1.59 ev

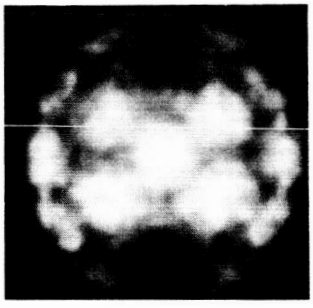

(f)

524° K
1.85 ev

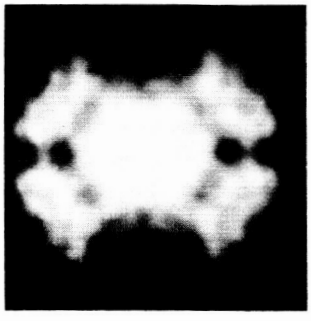

(g)

787° K
2.90 ev

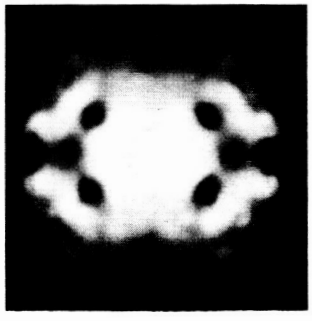

(h)

896° K
4.00 ev

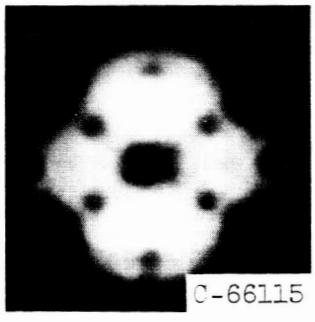

(i)

970° K
4.52 ev
Clean tungsten

Figure 6. - Sequence of field-emission patterns showing the thermal desorption of cesium deposited on clean tungsten as a function of substrate temperature. Successive patterns were obtained after heating for 60 seconds at temperatures indicated.

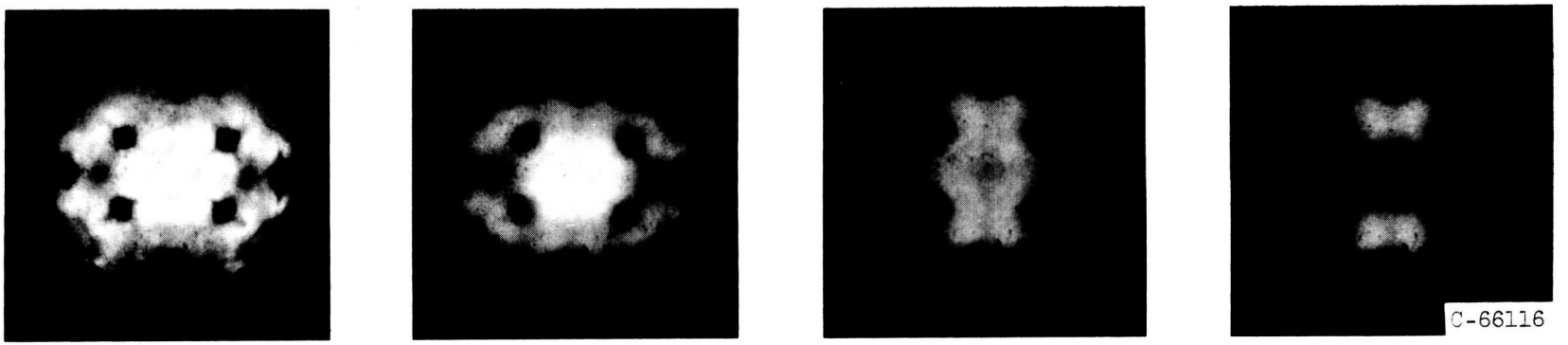

(a)
Average work function, 3.88 ev
Degree of adsorbate coverage, 0.07
Desorption time, 0 sec

(b)
Emitter surface temperature, 855° K
Desorption time, 225 sec

(c)
Emitter surface temperature, 855° K
Desorption time, 360 sec

(d)
Emitter surface temperature, 855° K
Degree of adsorbate coverage, 0
Desorption time, 450 sec

Figure 7. - Thermal desorption of cesium from tungsten observed with fixed-pulse viewing voltage of 5.0 kilovolts.

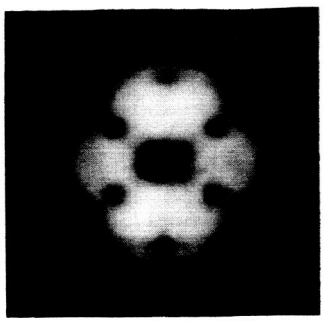

(a)

Clean tungsten

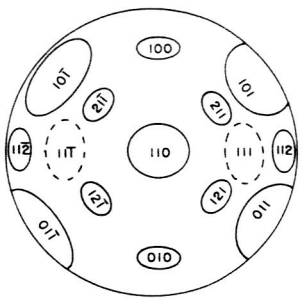

(b)

Diagram of principal planes of body-centered cubic pattern

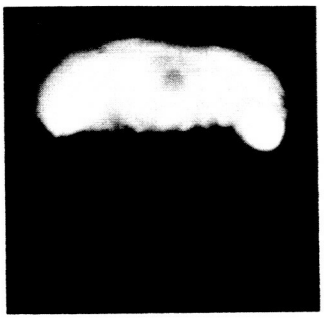

(c)

After evaporating cesium onto part of emitter (77° K)

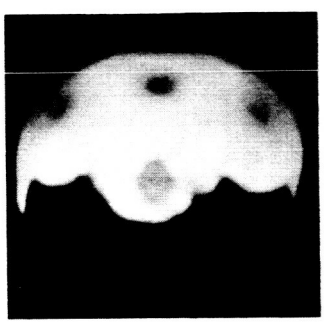

(d)

71 sec after heating to 187° K

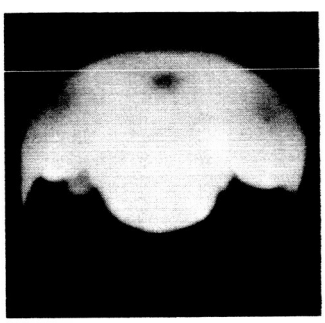

(e)

95 sec

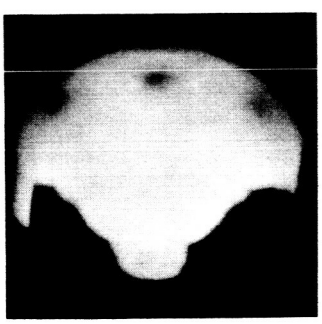

(f)

240 sec

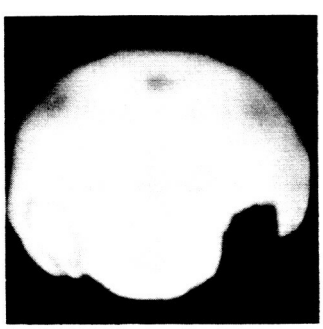

(g)

345 sec

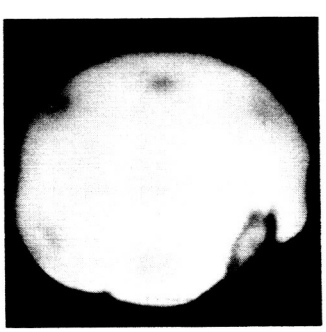

(h)

445 sec

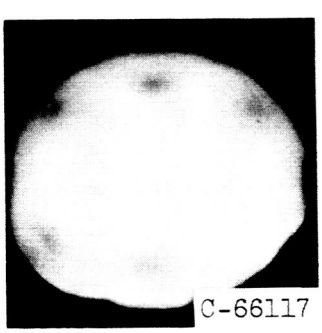

(i)

480 sec

Figure 8. - Pulsed-field-emission patterns illustrating surface migration of an initially heavy dose ($\theta > 1$) of cesium on tungsten emitter. Activation energy estimated at 6 kilocalories per mole.

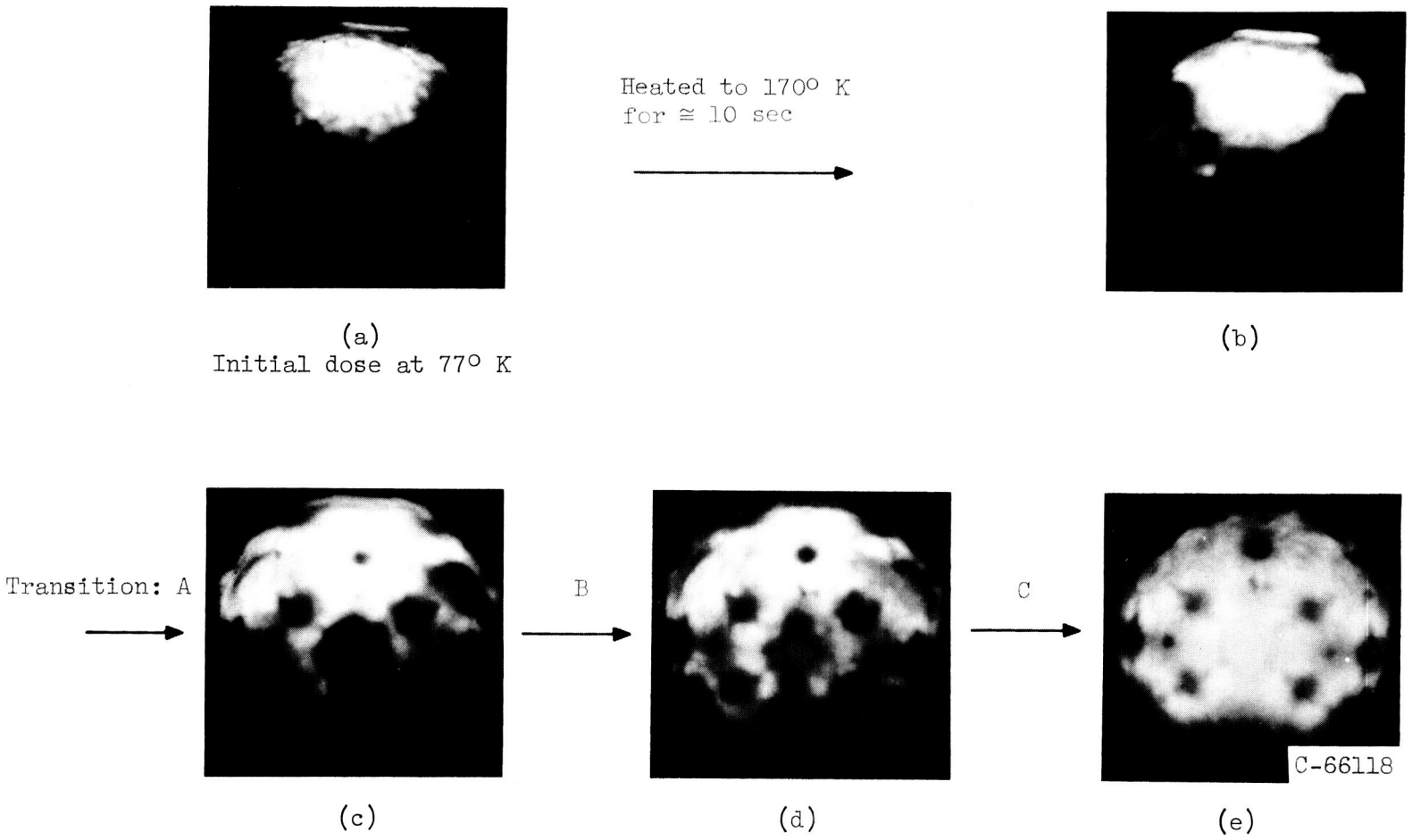

Figure 9. - Surface migration sequence of cesium on tungsten (initial degree of adsorbate coverage, ≅ 0.24). Activation energies measured for transitions A, B, and C are given in figure 11.

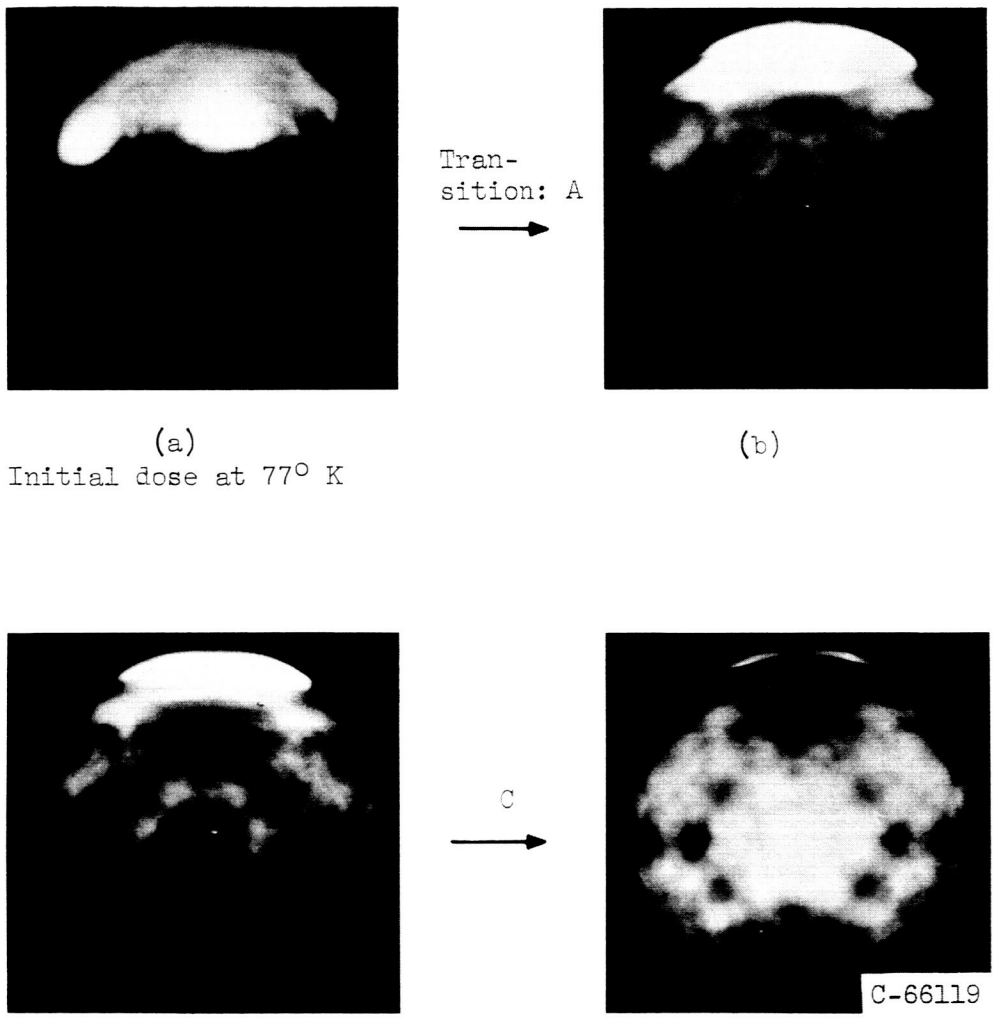

Figure 10. - Surface migration sequence of cesium on tungsten (initial degree of adsorbate coverage, ≅ 0.66). Note that the migration mode is the same as that at a smaller dose but with an additional receding boundary.

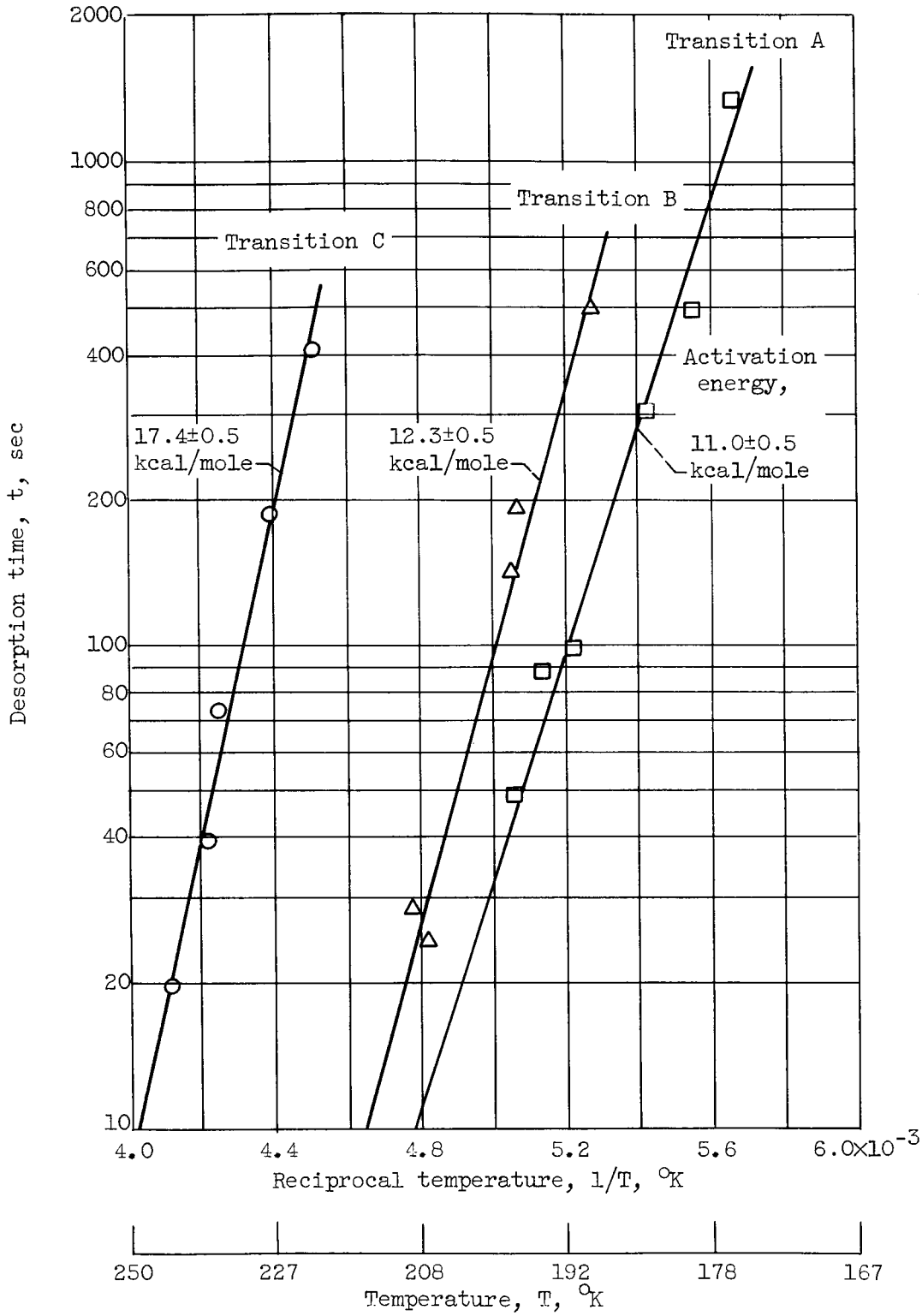

(a) Initial degree of absorbate coverage, ≅ 0.24.

Figure 11. - Arrhenius plots of surface migration data.

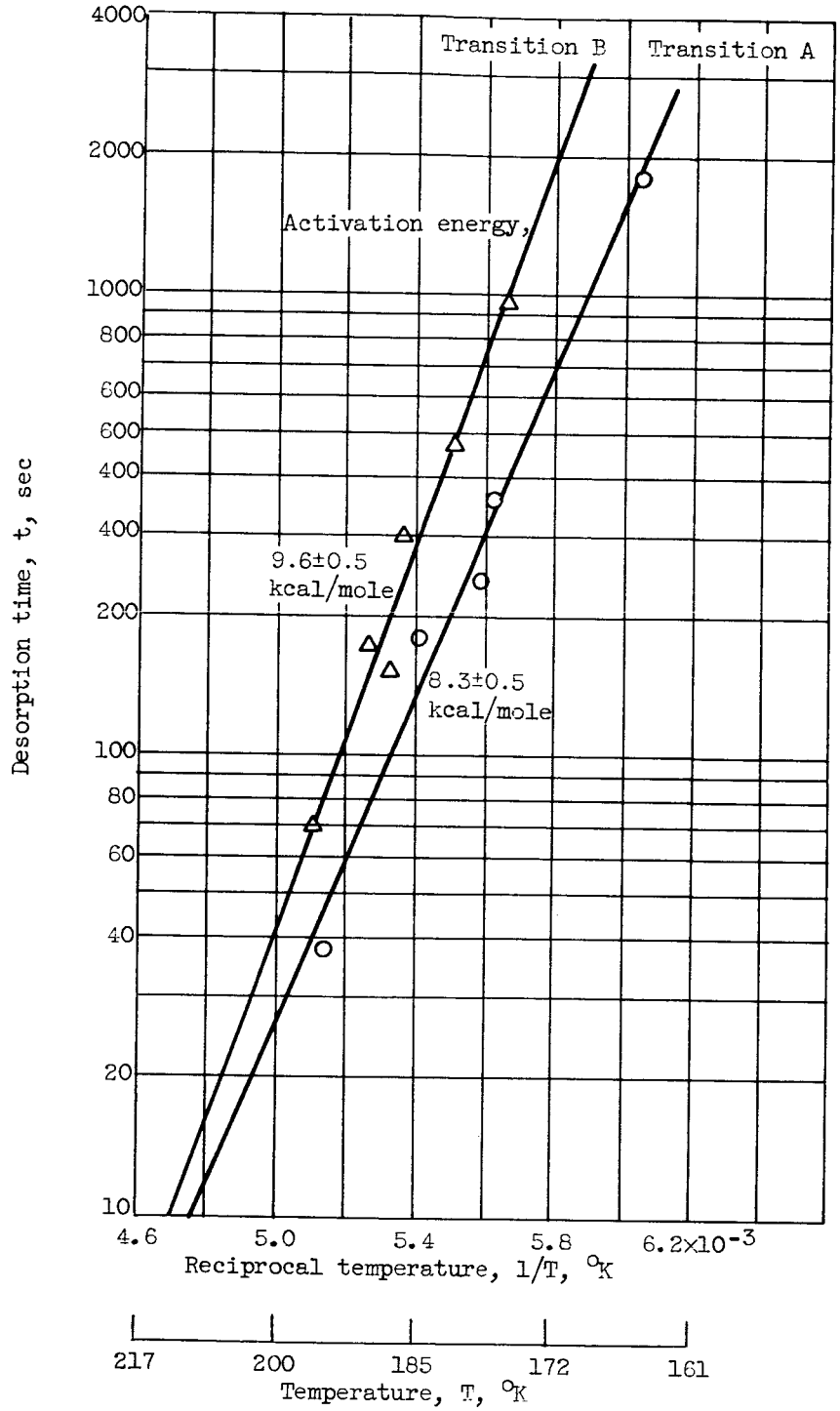

(b) Initial degree of adsorbate coverage, 0.08.

Figure 11. - Concluded. Arrhenius plots of surface migration data.

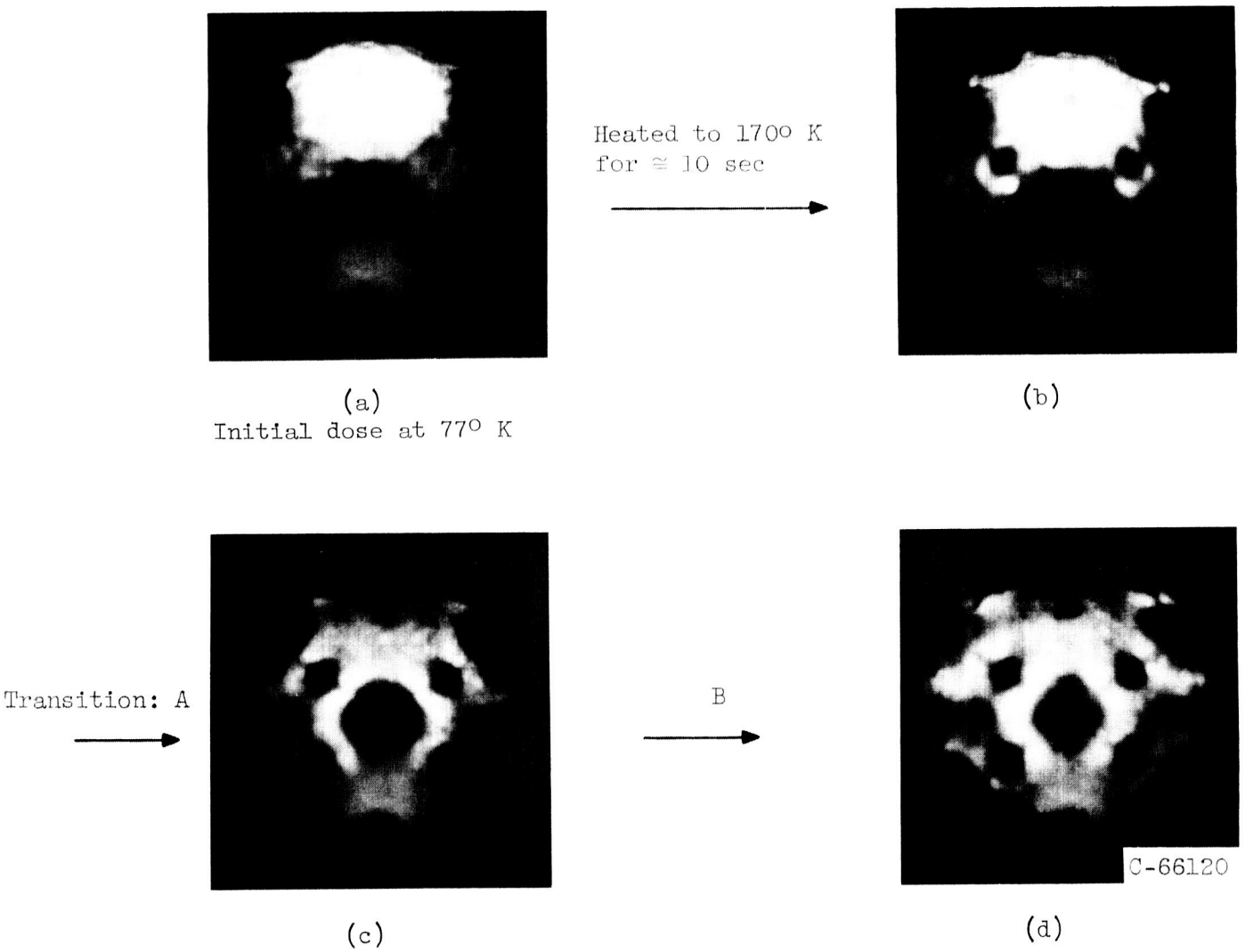

Figure 12. - Surface migration sequence of cesium on tungsten (initial degree of adsorbate coverage, ≅ 0.08). Activation energies measured for transitions A and B are given in figure 12.

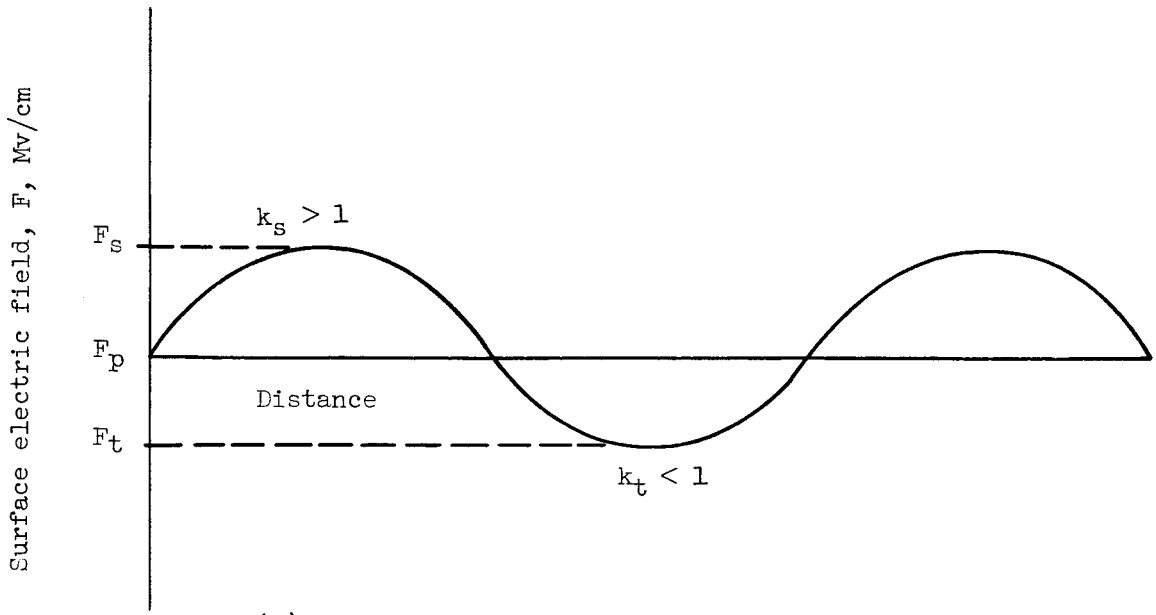

(a) Variation of field with distance along surface where F_p is the field at an ideally smooth surface, F_t the field on an adsorbate in the trough position, and F_s the field on an adsorbate migrating over the barrier.

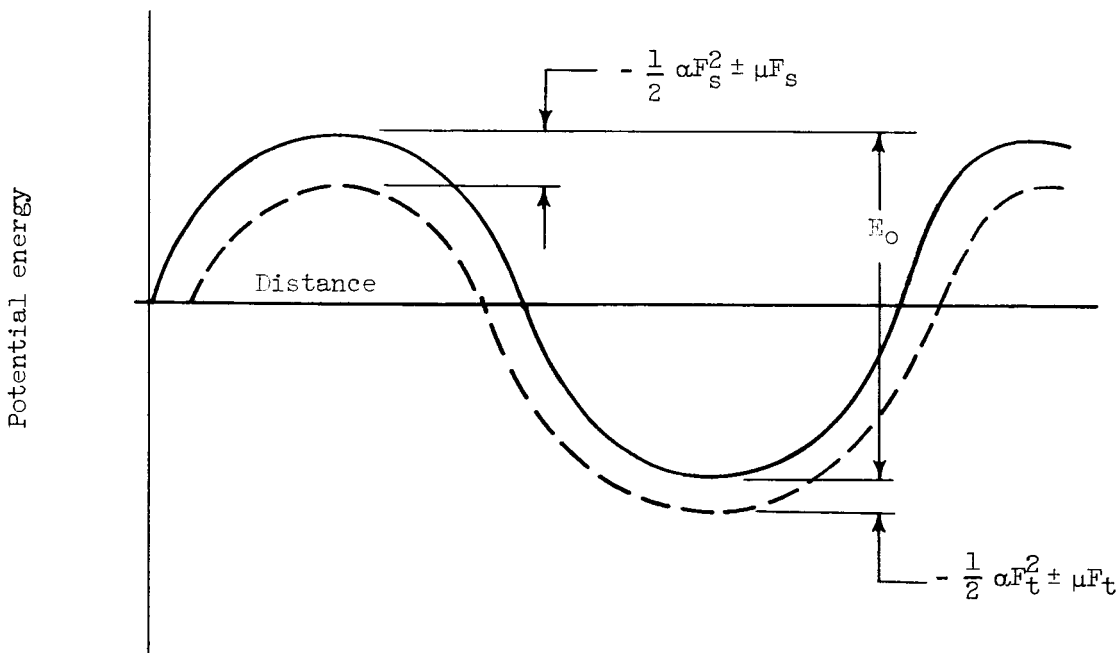

(b) Variation in potential valley depth and barrier height due to field-dipole and field-induced-dipole interactions.

Figure 13. - Model depicting effect of electric field on potential barrier for surface migration.

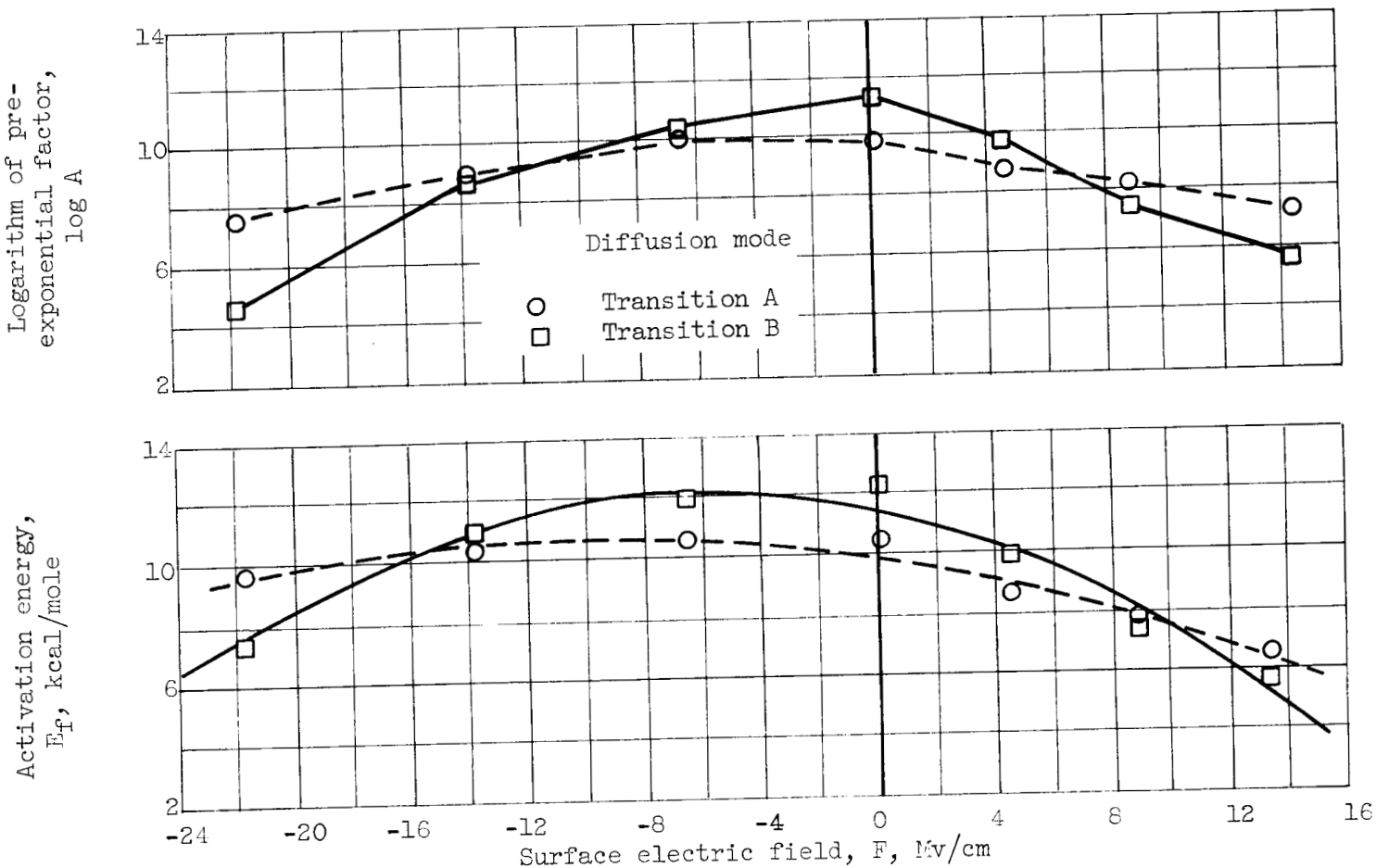

Figure 14. - Surface diffusion activation energy and logarithm of the pre-exponential factor as functions of electric field at emitter surface for the two diffusion modes in transitions A and B. The curves for activation energy are calculated from equation (11).

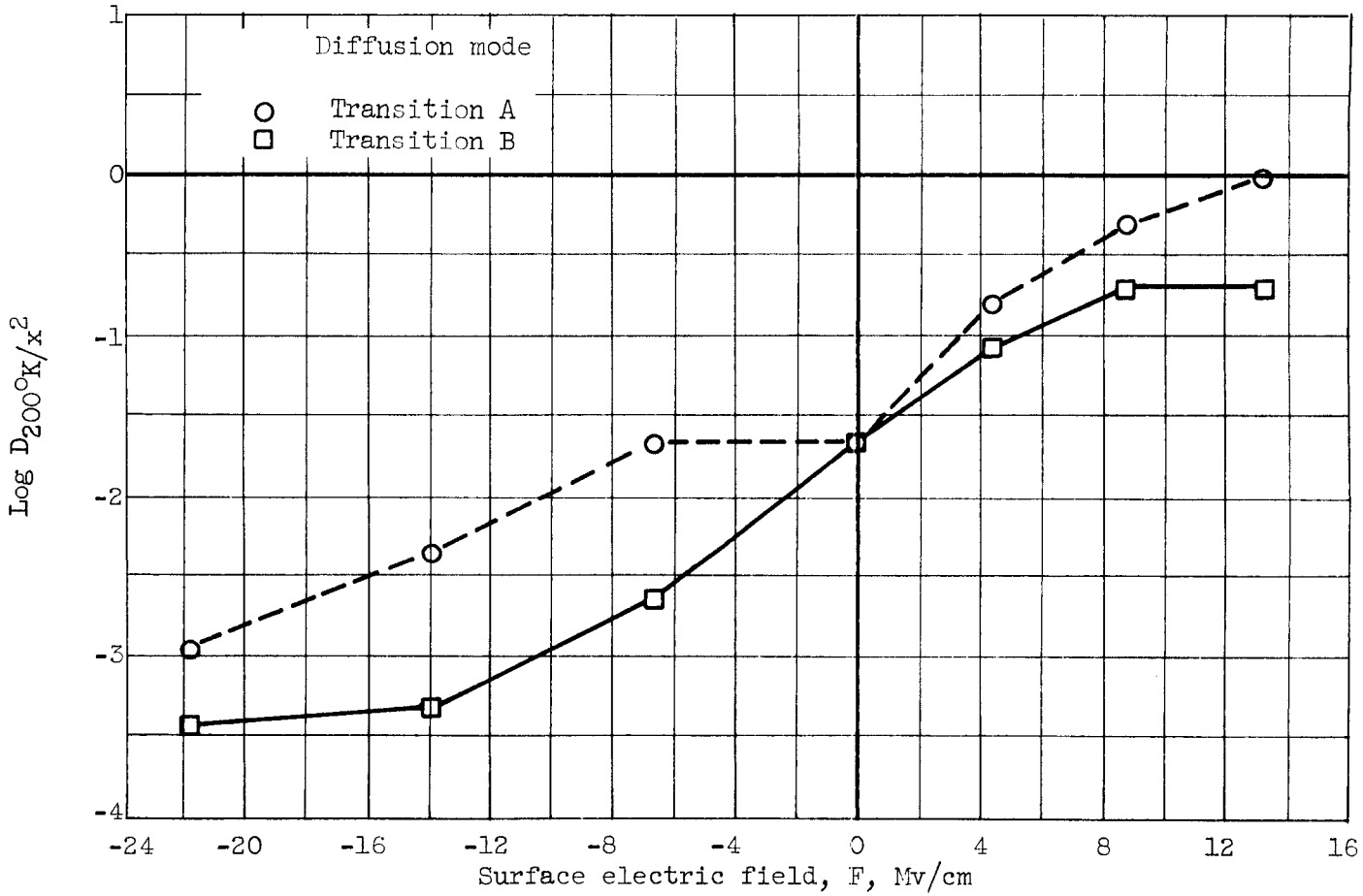

Figure 15. - Surface diffusion coefficient as a function of surface electric field for two diffusion modes in transitions A and B of cesium on tungsten at 200° K calculated from equation (8).

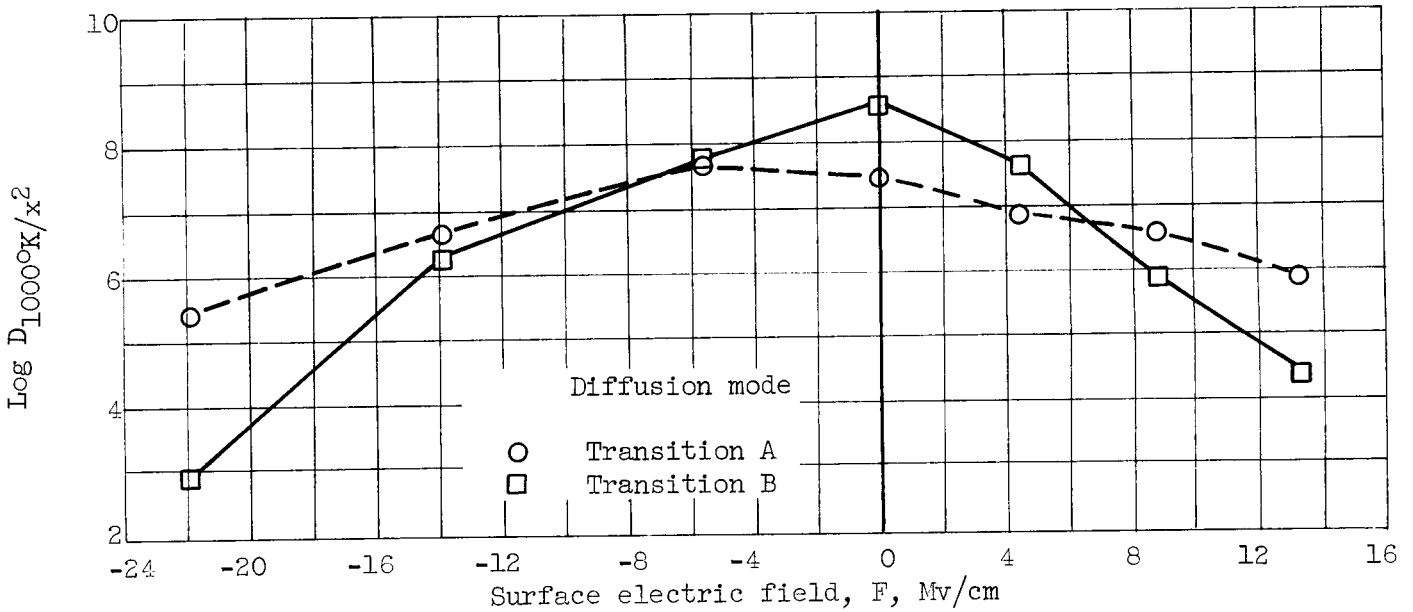

Figure 16. - Surface diffusion coefficient as a function of surface electric field for two diffusion modes in transitions A and B of cesium on tungsten at 1000° K calculated from equation (8).